Quantum Electrodynamics of Intense Laser-Matter Interactions: A Tool for Quantum State Engineering

AvH
Feodor
Lynen

MPG
MPI
Garching

Advanced ERC Grant:
NOQIA

Advanced ERC Grant:
QUAGATUA

Advanced ERC Grant:
OSYRIS

NeoST

Obra Social
Fundación "la Caixa"

CERCA/Program

Generalitat
de Catalunya

Quantum-Cat

EU FET-Open
OPTOlogic

OPTOlogic

SGR 1341

SGR 01452

FEDER/RIS3CAT

Quantum Electrodynamics of Intense Laser-Matter Interactions: A Tool for Quantum State Engineering

Symfonia

FNP
Polish Science Foundation

NCN
Narodowe Centrum Nauki

Fundació Privada
CELLEX

EXCELENCIA
SEVERO
OCHOA

FIDEUA

"Retos Colaboración" QUSPIN

GOBIERNO DE ESPAÑA
MINISTERIO DE CIENCIA E INNOVACIÓN

European Union NextGenerationEU (PRTR)

European Commission

Quantera
MAQS

Dynamite

Quantera
DYNAMITE

Fundació
Catalunya - La Pedrera

PASQuanS2

*iCrea
INSTITUCIÓ CATALANA DE RECERCA I ESTUDIS AVANÇATS

Unió Europea
Fons Europeu
Next Generation

GOBIERNO DE ESPAÑA

Plan de Recuperación, Transformación y Resiliencia

Next Generation
Catalunya

Generalitat de Catalunya
Departament de Recerca i Universitats

ICFO
Institut
de Ciències
Fotòniques

ICFO - Quantum Optics Theory (31 (7 females), 10 countries)

PhD ICFO (17)

Bárbara Andrade (many body, QI)
Niccolò Baldelli (many body, QI)
Mohit Lal Bera (QThermo)
David Cirauqui Garcia (MC optimization)
Gabriel Fernández Fernández (ML, QI)
Joana Fraxanet Morales (many body)
Aikaterini Gratsea (ML)
Adriano Macarone Palmieri (QI)

Guillem Müller Rigat (many body)
Eloy Piñol (ML, statphys)
Pavel Popov (many body)
Borja Requena Pozo (ML)
Tymoteusz Salamon (many body)
Anubhav Kumar Srivastava (QI, many body)
Philipp Stammer (atto)
Maria Recasens (many body/exp)
Yuma Watanabe (many body)

MSc/BSc ICFO (2)

David Pascual Solis (ML/many body)
Lingjian Liu (ML/many body)

Postdocs ICFO (12)

Dr. Utso Bhattacharya (many body, atto)
Dr. Przemysław Grzybowski (many body, ML)
Dr. Reiko Yamada (composer)
Dr. Marcin Plodzień (many body)
Dr. Grzegorz Rajchel-Mieldzioc (QI)
Dr. Piotr Sierant (many body)
Dr. Paolo Stornati (ML, QI, many body)
Dr. Lin Zhang (many body)
Dr. Themistoklis Mavrogordatos (QO)
Dr. Jessica Oliveira de Almeida (QO, QI)
Dr. Javier Argüello Luengo (many body)
Dr. Sourav Bhattacharee (many body)

Visiting professors, postocs, PhD

Prof. Ravindra Chhajlany (UAM)

Ex-members and collaborators: Aditi Sen De, Ujjwal Sen, Debraj Rakshit (HRI, Alahabad), Manab Bera (IIT), François Dubin (CNRS), G. John Lapeyre (IBM), Chiara Menotti (Trento), Jonas Larsson (Nordita), Philipp Hauke (Trento), Bruno Julia Díaz, Luca Tagliacozzo (UB), Anna Sanpera, Veronica Ahufinger, Alessio Celi (UAB), Tomek Sowiński, Mariusz Gada (IF PAN), Phillip Hauke (Trento), Omjyoti Dutta (GMV), Ralph Dum, Christian Trefzger (EC), Kuba Zakrzewski (UJ, Cracow), Boris Malomed (Haifa), Ulrich Ebling (Kyoto), Christine Muschik (UoT), Marek Kuś, Remigiusz Augusiak (CFT), Alexander Streltsov (UW), Ravindra Chhajlany, Przemek Grzybowski, Swapan Rana (ISI), Shi-Ju Ran (CNU), Irénée Frérot (Grenoble), Maria Maffei, Giulia de Rosi (UPC), Christos Charampoulos (IFICS), Angelo Piga (URiV), Zahra Khanian (TUM), Emilio Pisanty (KCL), Marcelo Ciappina (China-Technion), Titas Chanda, Emanuele Tirrito (SISSA), Luca Barbiero (Politecnica Torino), Alejandro Bermodez, Miguel Angel Martin-Delgado, German Sierra (Madrid), Albert Aloy (Vienna), Daniel González (Innsbruck), Luca Barbiero (Torino), Gorka Muñoz (Innsbruck), Simon Wall, Andy Maxwell (Aarhus), Tony Acín, Adrian Bachtold, Jens Biegert, Morgan Mitchell, Leticia Tarruell, Lluis Torner, Maria García-Parao (ICFO), Piotr Grochowski (Innsbruck), Jan Wehr (Tuscon). Paraskevas Tzallas, Theocharis Lamprou (FORTH), Anna Dawid (Flatiron), Alexandre Dauphin (PASCAL), Valenting Kasper (Sherbrook); Allan Johnson (Madrid), Tobias Grass (Donistia), Sergi Julià Farré (PASCAL)

Outline: Quantum Electrodynamics of Intense Laser-Matter Interactions: A Tool for Quantum State Engineering

Part I: "Standard" Super-Intense Laser-Matter Physics

0. General introduction
1. Strong field approximation (SFA) (on example of HHG)
2. Landau-Dykhne formula for HHG
3. Generalizations

Part II: Toward QED of Super-Intense Laser-Matter Physics

4. General introduction
5. Conditioning (on example of HHG)
6. Generalizations

ICFO
Institut de Ciències Fotòniques

Outline - Part I: "Standard Super-Intense Laser-Matter Physics

K. Amini et al., Symphony on Strong Field Approximation, Rep. Prog. Phys. 82 116001 (2019)

0. General introduction: QED of Super-Intense Laser-Matter Physics
    - 0.1 Generalities
    - 0.2 Processes
    - 0.3 Targets

1. Strong field approximation (SFA) (on example of HHG)
    - 1.1 Preliminaries
    - 1.2 Three step (simple man's) model
    - 1.3 Assumptions of SFA!!!

2. Landau-Dykhne formula for HHG (a.k.a. Lewenstein's model)
    - 2.1 Derivation
    - 2.2 Final expression
    - 2.3 Saddle point/stationary phase analysis
    - 2.4 Recovering simple man's model

3. Generalizations
    - 3.1 ATI (direct tunneling, re-scattering)
    - 3.2 NSDI – Electron Impact Ionization (EII)
    - 3.3 NSDI – Resonant Excitation Subsequent Ionization (RESI)
    - 3.4 Solids 3.5? Strongly correlated materials

ICFO Institut de Ciències Fotòniques

IOP Publishing Reports on Progress in Physics
Rep. Prog. Phys. **82** (2019) 116001 (42pp) https://doi.org/10.1088/1361-6633/ab2bb1

Review

Symphony on strong field approximation

Kasra Amini[1,2], Jens Biegert[2,3], Francesca Calegari[4,5], Alexis Chacón[6], Marcelo F Ciappina[7], Alexandre Dauphin[2], Dmitry K Efimov[8], Carla Figueira de Morisson Faria[9], Krzysztof Giergiel[8], Piotr Gniewek[1], Alexandra S Landsman[10,11], Michał Lesiuk[1], Michał Mandrysz[8], Andrew S Maxwell[9], Robert Moszyński[1], Lisa Ortmann[12], Jose Antonio Pérez-Hernández[13], Antonio Picón[2,14], Emilio Pisanty[2], Jakub Prauzner-Bechcicki[8], Krzysztof Sacha[8,15], Noslen Suárez[2], Amelle Zaïr[16], Jakub Zakrzewski[8,15] and Maciej Lewenstein[2,3]

[1] Faculty of Chemistry, University of Warsaw, Pasteura 1, 02-093 Warsaw, Poland
[2] ICFO—Institut de Ciencies Fotoniques, The Barcelona Institute of Science and Technology, 08860 Castelldefels (Barcelona), Spain
[3] ICREA, Pg. Lluís Companys 23, 08010 Barcelona, Spain
[4] Center for Free-Electron Laser Science, DESY, Notkestr. 85, 22607 Hamburg, Germany
[5] CNR, Instituto di Fotonica e Nanotecnologie Milano, Piazza L. da Vinci 32, 20133 Milano, Italy
[6] Center for Nonlinear Studies and Theoretical Division, Los Alamos National Laboratory, Los Alamos, NM 87545, United States of America
[7] Institute of Physics of the ASCR, ELI-Beamlines project, Na Slovance 2, 182 21 Prague, Czech Republic
[8] Instytut Fizyki imienia Mariana Smoluchowskiego, Uniwersytet Jagielloński, Łojasiewicza 11, 30-348 Kraków, Poland
[9] Department of Physics & Astronomy, University College London, Gower Street, London WC1E 6BT, United Kingdom
[10] Max-Planck Institut für Physik Komplexer Systeme, Nöthnitzer-Strasse 38, D-01187 Dresden, Germany
[11] Department of Physics, Max Planck Postech, Pohang, Gyeongbuk 37673, Republic of Korea
[12] Max-Planck Institut für Physik komplexer Systeme, Nöthnitzer-Strasse 38, D-01187 Dresden, Germany
[13] Centro de Láseres Pulsados (CLPU), Parque Científico, E-37185 Villamayor, Salamanca, Spain
[14] Departamento de Química, Universidad Autónoma de Madrid, 28049, Madrid, Spain
[15] Mark Kac Complex Systems Research Center, Jagiellonian University, Łojasiewicza 11, 30-348 Kraków, Poland
[16] King's College London, Department of Physics, London WC2R 2LS, United Kingdom

E-mail: maciej.lewenstein@icfo.eu

Received 8 February 2019, revised 20 May 2019
Accepted for publication 21 June 2019
Published 14 October 2019

Corresponding Editor Professor Masud Mansuripur

PHYSICAL REVIEW A VOLUME 49, NUMBER 3 MARCH 1994

Theory of high-harmonic generation by low-frequency laser fields

M. Lewenstein,[1,*] Ph. Balcou,[2] M. Yu. Ivanov,[3,†] Anne L'Huillier,[2,4] and P. B. Corkum[3]
[1]*Joint Institute for Laboratory Astrophysics, University of Colorado, Boulder, Colorado 80309-0440*
[2] *Service des Photons, Atomes et Molécules, Centre d'Etudes de Saclay, 91191 Gif sur Yvette, France*
[3]*National Research Council of Canada, M-23A, Ottawa, Ontario, Canada K1A OR6*
[4]*Lawrence Livermore National Laboratory, L-443, P.O. Box 5508, Livermore, California 94550*
(Received 19 August 1993)

We present a simple, analytic, and fully quantum theory of high-harmonic generation by low-frequency laser fields. The theory recovers the classical interpretation of Kulander *et al.* in [*Proceedings of the SILAP III Workshop*, edited by B. Piraux (Plenum, New York, 1993)] and Corkum [Phys. Rev. Lett. **71**, 1994 (1993)] and clearly explains why the single-atom harmonic-generation spectra fall off at an energy approximately equal to the ionization energy plus about three times the oscillation energy of a free electron in the field. The theory is valid for arbitrary atomic potentials and can be generalized to describe laser fields of arbitrary ellipticity and spectrum. We discuss the role of atomic dipole matrix elements, electron rescattering processes, and of depletion of the ground state. We present the exact quantum-mechanical formula for the harmonic cutoff that differs from the phenomenological law $I_p + 3.17U_p$ where I_p is the atomic ionization potential and U_p is the ponderomotive energy, due to the account for quantum tunneling and diffusion effects.

PACS number(s): 42.65.Ky, 32.80.Rm

Feature

50 Years of *Physical Review A*: The Legacy of Three Classics

March 2, 2020• *Physics* 13, 24

Physicists working in optics, atomic and molecular physics, and quantum information reflect on landmark papers and how they influence research today.

0. General introduction

0.1 General introduction: Generalities

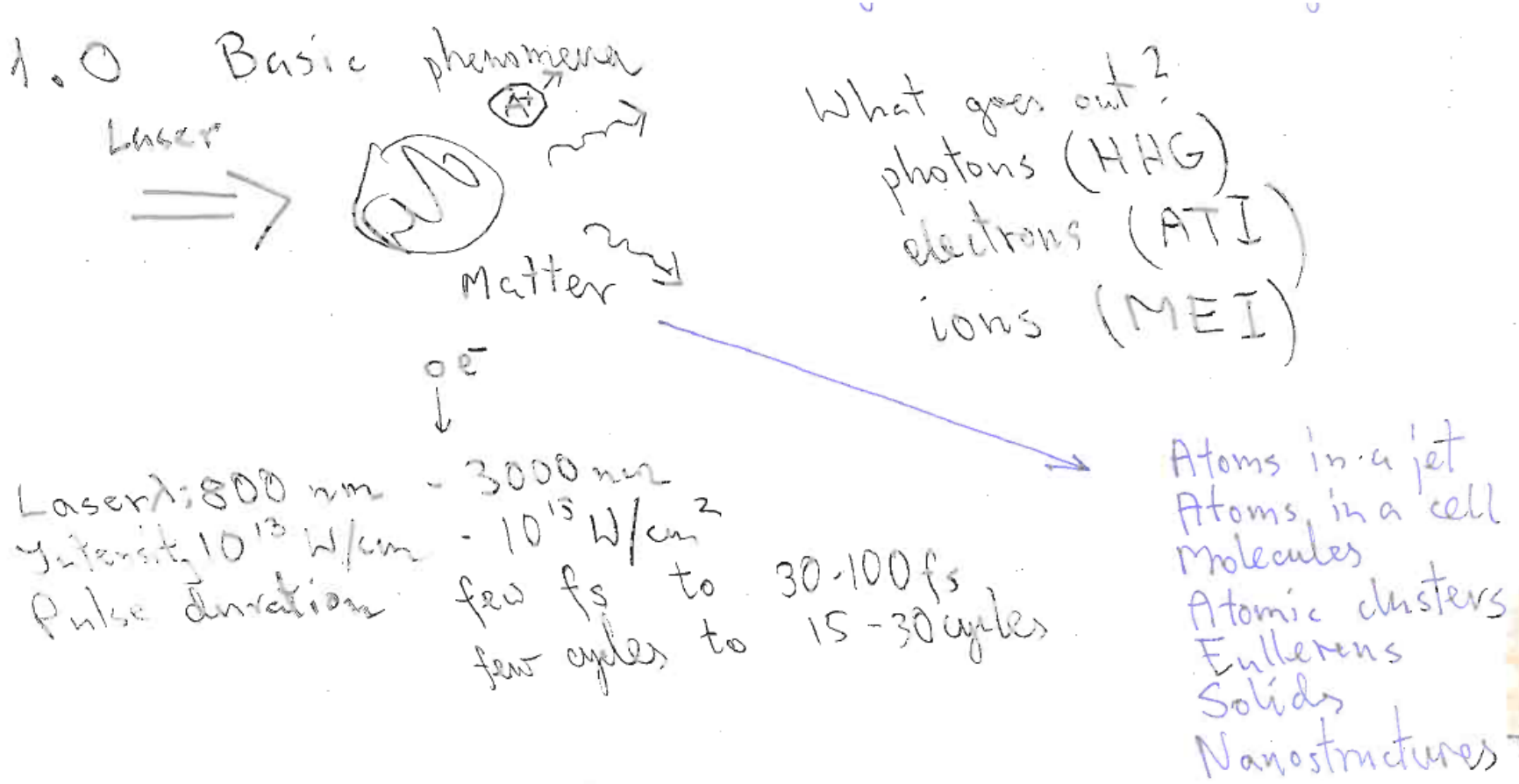

0.2 - General introduction: Processes

Rep. Prog. Phys. **82** (2019) 116001

Table 1. The operating conditions in terms of photon energy, $\hbar\omega$, ionization potential, I_p, and ponderomotive energy, U_p are presented for single-photon ionization (SPI), multi-photon ionization (MPI), above-threshold ionization (ATI) and tunnel ionization (TI).

Ionization regime	Operating condition
Single-photon ionization (SPI)	$\hbar\omega > I_p \gg U_p$
Multi-photon ionization (MPI)	$I_p > \hbar\omega \gg U_p$
Above-threshold ionization (ATI)	$I_p > U_p > \hbar\omega$
Tunnel ionization (TI)	$U_p > I_p > \hbar\omega$

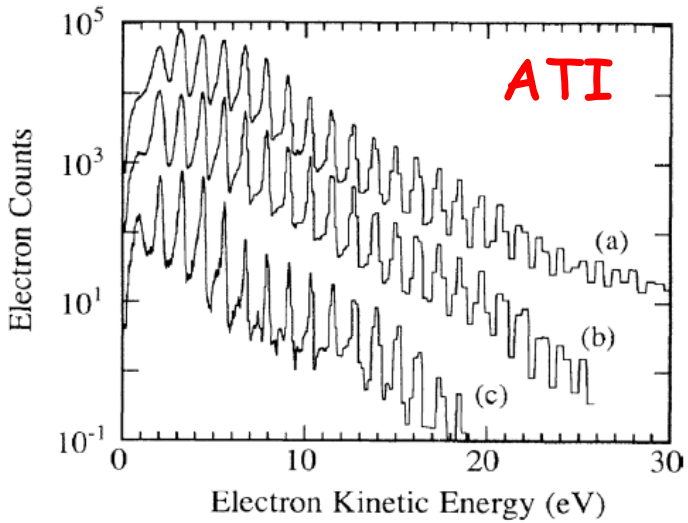

Figure 2. Above-threshold ionization (ATI) spectrum of xenon illuminated with a 50 ps, 1.05 μm laser pulse at three intensities: (a) 2.0×10^{13} W cm^{-2}, (b)1.5×10^{13} W cm^{-2}, and (c) 1.0×10^{13} W cm^{-2}. Reprinted figure with permission from [81], Copyright (1993) by the American Physical Society.

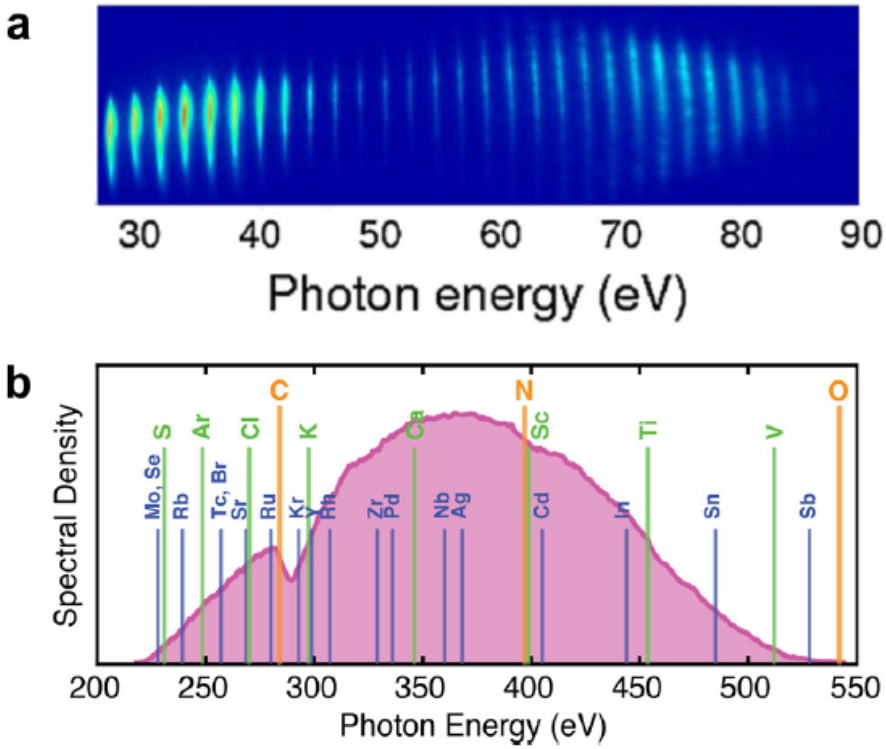

Figure 3. HHG spectrum for (a) a train of attosecond pulses and (b) an isolated attosecond pulse. In panel (a), argon was illuminated with a 40 fs (10-cycle), 1200 nm driving laser pulse to generate a spectrum over the 30–90 eV range. In panel (b), helium was ionized by a 12 fs (1.8-cycle), 1850 nm laser pulse to generate a broadband spectrum over the entire water window range of 284–543 eV, with the K- (orange), L- (green), and M-shell (blue) absorption edges indicated by vertical lines. (a) Reproduced from [241]. © IOP Publishing Ltd. All rights reserved. (b) (c) 2018 Optical Society of America, and it is reproduced from Ref. [242].

HHG

0.2 - General introduction: Processes

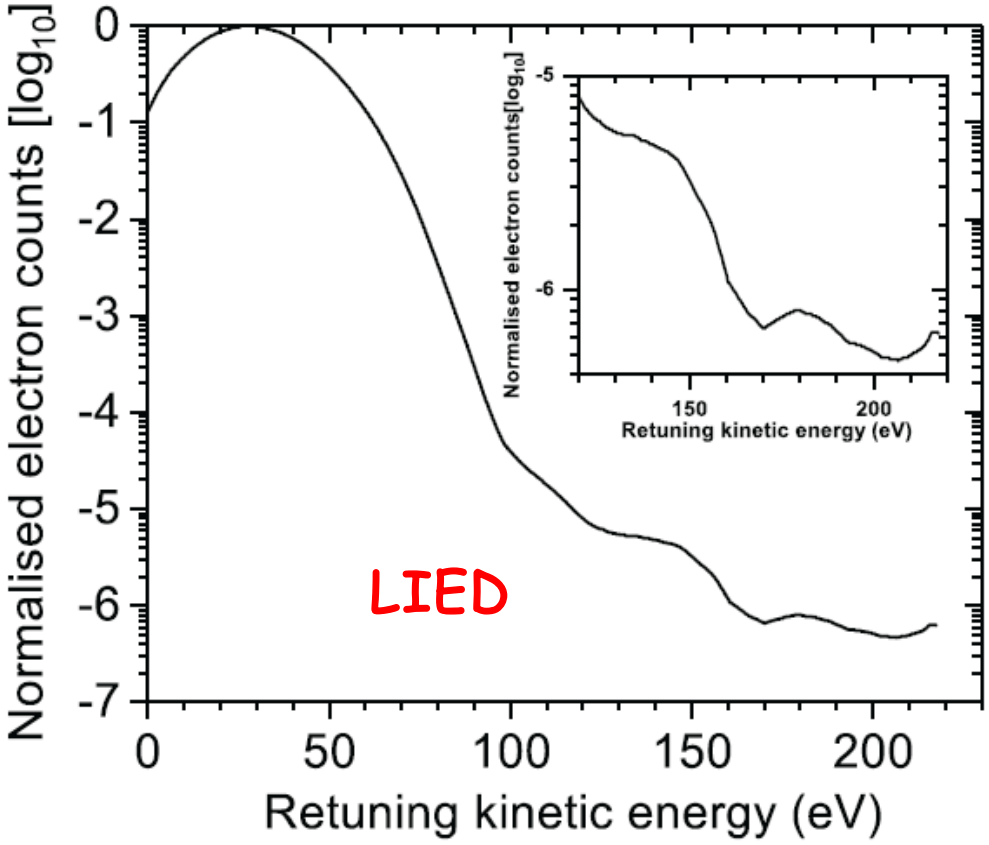

Figure 5. Typical photoelectron spectrum recorded with LIED of $C_2H_2^+$, with the direct photoelectrons (<3.5 a.u.) and rescattered electrons (>3.5 a.u.) present. Oscillations are clearly seen in the rescattered energy range of the electron signal that is a result of the coherent molecular interference signal which is dependent on the target's geometric structure. The inset shows a zoomed-in view of the oscillations in the differential cross-section of the scattering energy range. Reproduced from [251]. CC BY 4.0.

ICFO Institut de Ciències Fotòniques

MEI (SDI, NSDI: EII, RESI)

Rep. Prog. Phys. **82** (2019) 116001 Review

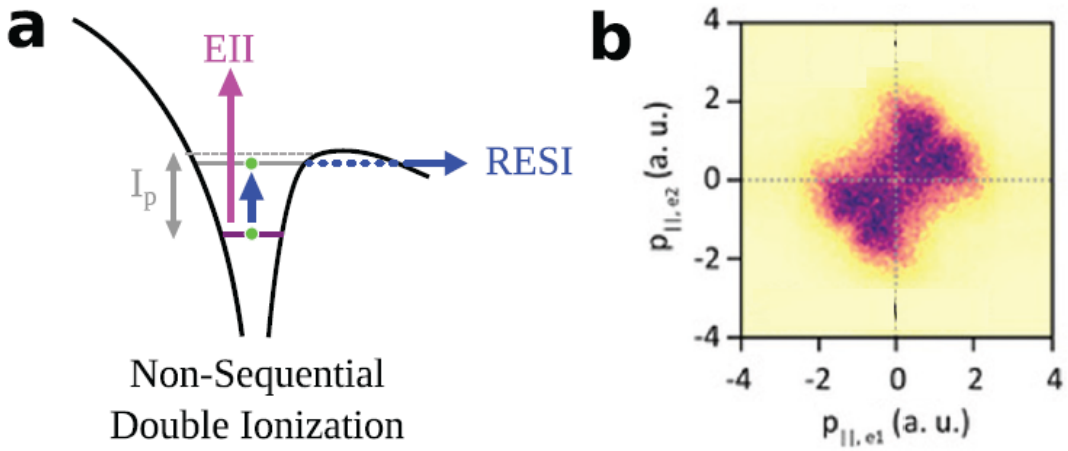

Figure 4. (a) Non-sequential double ionization (NSDI) illustrated after the recollision of e_1 with the target ion using an atomic Coulomb potential. After inelastic recollision, either the second electron is ejected through: (i) an electron-impact process (pink arrow) or (ii) excited and subsequently ionized through recollision-excitation with subsequent ionization (RESI; blue arrow). (b) The typical EII signature in a two-dimensional momentum map $(p_{\|,1}, p_{\|,2})$ of the longitudinal momenta of the two electrons in atomic units (a.u.) from strong-field ionized Xe^{2+} ions. (In contrast, RESI may lead to a myriad of shapes in correlated electron–electron distributions, and in principle occupies all four quadrants.) (b) Reprinted figure with permission from [249], Copyright (2017) by the American Physical Society.

Targets

- Atoms in a jet
- Atoms in a cell
- Simple molecules
- Large, complex molecules
- Atomic clusters
- Fullerens
- Liquids
- "Standard" solids
- Topological materials
- Strongly correlated materials
- 2D materials
- 1D quantum wires …

1. Strong Field Approximation

1.1 – Strong field approximation: Preliminaries

The TDSE reads:

Single active electron approximation (SAE), dipole approximation

$$i\hbar\frac{\partial}{\partial t}|\Psi(t)\rangle = \hat{H}|\Psi(t)\rangle, \tag{4}$$

where the Hamiltonian, $\hat{H}$, describes the laser-target syst
in SAE approximation, and is the sum of two terms, i

$$\hat{H} = \hat{H}_0 + \hat{U}, \tag{5}$$

where $\hat{H}_0$ is the laser-free Hamilt he atomic or

$$\mathbf{E}(t) = \mathcal{E} \quad (\omega_0 t + \phi_0)\,\mathbf{e}_z.$$

$\mathcal{E}_0\mathbf{e}_z \rightarrow \mathbf{E}_0(t)$. $\quad \hat{} \quad \frac{}{2m} + V(\hat{\mathbf{r}}), \tag{6}$

with $V(\hat{\mathbf{r}})$ ive SAE atomic or molecular potential, m the mass, and $\hat{U} = -e\mathbf{E}(t)\cdot\hat{\mathbf{r}}$ the dipole coupling, wh escribes the interaction of the atomic or molecular system with the laser radiation, written in the length gauge

Strong EM field is treated classically!!!

1.2 – Strong field approximation: Simple man's model

(3) 1.1.2 HHG — P. Corkum – K. Kulander (K. Schafer, J. Krause)

Position of the cutoff $I_p + 3.2\,U_p$

Simple man's / Three step model

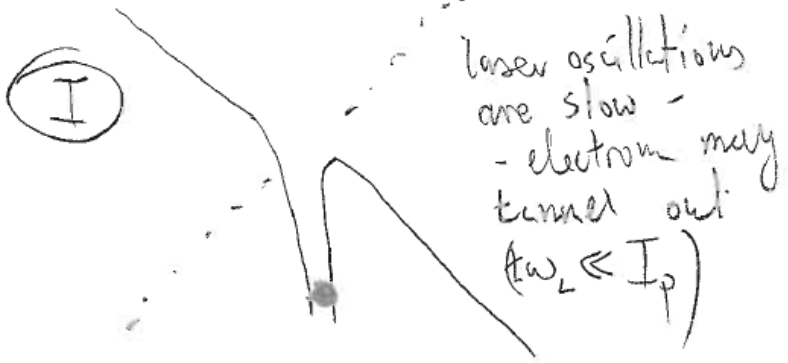

II

electron oscillates in $\mathcal{E}(t)$ essentially not feeling the nucleus ($U_p \gg I_p, \hbar\omega_L$)

III

electron recombines to the ground state and large energy photon is emitted.

How much energy can electron get?

Purely classical problem!

maximal kinetic energy gain $\simeq 3.2\,U_p$!

1.3 – Strong field approximation: Assumptions!!!

(i) The strong field laser does not couple with any bound state beyond the ground state, $|0\rangle$, so that only it and the continuum (scattering) states, $|\mathbf{p}\rangle$, are taken into account in the dynamics;

(ii) The amplitude of the ground state, $a(t)$, is considered to be known.

(iii) The continuum states are taken from the basis of *exact* scattering states, which are eigenstates via

$$\hat{H}_0|\mathbf{p}\rangle = \frac{1}{2m}\mathbf{p}^2|\mathbf{p}\rangle \tag{7}$$

of the atomic Hamiltonian with a fixed outgoing (kinetic) momentum $\mathbf{p}$. The continuum–continuum matrix element from $\mathbf{p}$ to $\mathbf{p}'$ are then decomposed into their most singular part, proportional to $i\hbar\nabla_{\mathbf{p}}\delta(\mathbf{p}-\mathbf{p}')$, and the 'rest' [29, 58, 113]. The 'rest' is then treated in a perturbative manner [29].

1.3 – Strong field approximation: Assumptions!!!

Ad (i) Based on the statement (i), the electronic state $|\Psi(t)\rangle$ that represents the time evolution of the system is a coherent superposition of the ground $|0\rangle$ and the continuum $|\mathbf{p}\rangle$ states [29, 113]:

$$|\Psi(t)\rangle = \mathrm{e}^{\mathrm{i}I_p t/\hbar}\left(a(t)|0\rangle + \int \mathrm{d}^3\mathbf{p}\; b(\mathbf{p},t)|\mathbf{p}\rangle\right). \qquad (8)$$

The factor $a(t)$, representing the amplitude of the ground state, is assumed to be known (see below for the ways to evaluate or estimate it). The prefactor $\mathrm{e}^{\mathrm{i}I_p t/\hbar}$ represents the phase oscillations which describe the accumulated electron energy in the ground state ($I_p = -E_0$ is the ionization potential, with E_0 the ground-state energy of the target system). Furthermore, the transition amplitude to the continuum states is denoted by $b(\mathbf{p},t)$, and it depends both on the kinetic momentum of the outgoing electron and the laser pulse. Note that, if needed, other (relevant) bound states may be taken into account in the expression (8) (see [263], [104, 168]).

1.3 – Strong field approximation: Assumptions!!!

Ad (ii) There are several ways of evaluating or estimating $a(t)$, depending on the regime of parameters.

- Using TDSE
- Using phase space averaging/truncated Wigner
- Using ADK rates
- Setting a(t) ~ 1
- Using SFA itself
- …

1.3 – Strong field approximation: Assumptions!!!

Ad (iii) The continuum–continuum matrix element, independently of the fact whether the effective SAE potential is short-range (as it is for model atoms and negative ions) or Coulomb-like, has the general form:

$$e\langle \mathbf{p}|\hat{\mathbf{r}}|\mathbf{p}'\rangle = \mathrm{i}e\hbar\nabla_{\mathbf{p}}\delta(\mathbf{p}-\mathbf{p}') + \hbar\mathbf{g}(\mathbf{p},\mathbf{p}'), \tag{9}$$

where the part $\hbar\mathbf{g}(\mathbf{p},\mathbf{p}')$ is less singular—typically the strongest singularity it contains corresponds to the on-energy-shell gradient of the Dirac delta of $\mathbf{p}^2-(\mathbf{p}')^2$. This part is responsible for rescattering effects in ATI and recollisions in NSMI. Note that since we insist on using the *exact* scattering states, the dipole matrix element $\langle \mathbf{p}|\hat{\mathbf{r}}|0\rangle$ (together with the rescattering continuum–continuum matrix elements) does include the full effects of the effective SAE potential, comprising both the short-range effects as well as any long-range Coulomb effects (if present).

Note also that the SFA in the present formulation (actually equivalent to that of [29]) does not involve plane waves or Volkov solutions! The majority of authors, including ourselves, 'erroneously' (in the view of the present formulation) claim that SFA corresponds to the use of Volkov states in the continuum. This is, in principle, false and dangerous. One can use additional approx-

2. Landau-Dykhne formula for HHG

2.1 – Landau-Dykhne formula for HHG: Derivation

$$\dot{a}(t) = \frac{\mathrm{i}}{\hbar} \int \mathrm{d}^3\mathbf{p}\, \mathbf{E}(t) \cdot \mathbf{d}^*(\mathbf{p})\, b(\mathbf{p}, t) \tag{10}$$

$$\dot{b}(\mathbf{p}, t) = -\frac{\mathrm{i}}{\hbar}\left(\frac{\mathbf{p}^2}{2m} + I_p\right) b(\mathbf{p}, t) + \frac{\mathrm{i}}{\hbar}\mathbf{E}(t) \cdot \mathbf{d}(\mathbf{p}) a(t)$$
$$- e\mathbf{E}(t) \cdot \nabla_{\mathbf{p}} b(\mathbf{p}, t) + \mathrm{i}\mathbf{E}(t) \cdot \int \mathrm{d}^3\mathbf{p}'\, b(\mathbf{p}', t)\mathbf{g}(\mathbf{p}, \mathbf{p}'). \tag{11}$$

$$e\langle \mathbf{p}|\hat{\mathbf{r}}|0\rangle = \mathbf{d}(\mathbf{p}). \tag{12}$$

ICFO
Institut de Ciències Fotòniques

2.1 – Landau-Dykhne formula for HHG: Derivation

zeroth order solution:

$$\partial_t b_0(\mathbf{p},t) = -\frac{\mathrm{i}}{\hbar}\left(\frac{\mathbf{p}^2}{2m}+I_p\right) b_0(\mathbf{p},t) + \frac{\mathrm{i}}{\hbar}\,\mathbf{E}(t)\cdot\mathbf{d}(\mathbf{p})a(t) + e\mathbf{E}(t)\cdot\nabla_{\mathbf{p}} b_0(\mathbf{p},t). \quad (14)$$

$$b_0(\mathbf{p},t) = \frac{\mathrm{i}}{\hbar}\int_0^t \mathrm{d}t'\,\mathbf{E}(t')\cdot\mathbf{d}\left(\mathbf{p}+e\mathbf{A}(t)/c - e\mathbf{A}(t')/c\right) \times \exp\left(-\mathrm{i}\int_{t'}^t \mathrm{d}\tilde{t}\left[\frac{1}{2m}(\mathbf{p}+e\mathbf{A}(t)/c - e\mathbf{A}(\tilde{t})/c)^2 + I_p\right]/\hbar\right) a(t'). \quad (15)$$

2.1 – Landau-Dykhne formula for HHG: Derivation

$$b_0(\mathbf{p},t) = \frac{\mathrm{i}}{\hbar}\int_0^t \mathrm{d}t'\,\mathbf{E}(t')\cdot\mathbf{d}\left(\mathbf{p}-e\mathbf{A}(t')/c\right)a(t') \times \exp\left(-\mathrm{i}\int_{t'}^{t}\mathrm{d}\tilde{t}\left[\frac{1}{2m}\left(\mathbf{p}-e\mathbf{A}(\tilde{t})/c\right)^2+I_p\right]/\hbar\right). \quad (16)$$

Where the quasi-classical action is:

$$S(\mathbf{p},t,t') = \int_{t'}^{t}\mathrm{d}\tilde{t}\left[\frac{1}{2m}\left(\mathbf{p}-e\mathbf{A}(\tilde{t})/c\right)^2+I_p\right]. \quad (17)$$

ICFO
Institut de Ciències Fotòniques

2.2 – Landau-Dykhne formula for HHG: Final expression

$$< \mathbf{r}(t) > = \mathrm{Re}\{\int \mathrm{d}^3\mathbf{p}\ \mathbf{d}(\mathbf{p})\ a(t) b(\mathbf{p},t)\}$$

$$\langle \mathbf{r}(t) \rangle = \mathrm{Re}\left[\frac{\mathrm{i}}{\hbar} \int_0^t \mathrm{d}t' \int \mathrm{d}^3\mathbf{p}\, a^*(t) \mathbf{d}^*(\mathbf{p} - e\mathbf{A}(t)/c) \right.$$
$$\mathbf{E}(t') \cdot \mathbf{d}\,(\mathbf{p} - e\mathbf{A}(t')/c)\, a(t') \times$$
$$\left. \exp\left(-\mathrm{i} \int_{t'}^t \mathrm{d}\tilde{t} \left[\frac{1}{2m} (\mathbf{p} - e\mathbf{A}(\tilde{t})/c)^2 + I_p \right] / \hbar \right) \right], \quad (21)$$

ICFO
Institut de Ciències Fotòniques

2.2 – Landau-Dykhne formula for HHG: Final expression

$$\tilde{\mathbf{r}}(\Omega) = \int_{-\infty}^{\infty} \langle \mathbf{r}(t) \rangle \mathrm{e}^{+\mathrm{i}\Omega t} \mathrm{d}t = \mathrm{Re}\left[\frac{\mathrm{i}}{\hbar} \int_{-\infty}^{\infty} \mathrm{d}t \right.$$
$$\int_0^t \mathrm{d}t' \int \mathrm{d}^3\mathbf{p}\, a^*(t) \mathbf{d}^*(\mathbf{p} - e\mathbf{A}(t)/c) \mathbf{E}(t') \cdot \mathbf{d}(\mathbf{p} - e\mathbf{A}(t')/c)\, a(t')$$
$$\left. \times \exp\left(-\mathrm{i} \int_{t'}^{t} \mathrm{d}\tilde{t} \left[\frac{1}{2m} (\mathbf{p} - e\mathbf{A}(\tilde{t})/c)^2 + I_p \right] / \hbar + \mathrm{i}\Omega t \right) \right], \qquad (22)$$

where Ω is the frequency of the emitted harmonic.

ICFO
Institut de Ciències Fotòniques

2.3 – Landau-Dykhne formula for HHG: Saddle point analysis

$$\frac{\partial}{\partial t'} S_{\Omega}(\mathbf{p}, t, t') = \frac{1}{2m}(\mathbf{p} - e\mathbf{A}(t')/c)^2 + I_p = 0 \tag{24}$$

$$\frac{\partial}{\partial t} S_{\Omega}(\mathbf{p}, t, t') + \Omega = \frac{1}{2m}(\mathbf{p} - e\mathbf{A}(t)/c)^2 + I_p = \hbar\Omega \tag{25}$$

$$\nabla_{\mathbf{p}} S_{\Omega}(\mathbf{p}, t, t') = \frac{1}{m}\int_{t'}^{t} [\mathbf{p} - e\mathbf{A}(\tilde{t})/c]\, \mathrm{d}\tilde{t} = 0 \tag{26}$$

2.3 – Landau-Dykhne formula for HHG: Recovering simple man's model

Within that steepest-descent approximation, then, SFA amplitudes are given by a sum over all the relevant saddle-point roots that contribute to the deformed integration contour,

$$\tilde{\mathbf{r}}(\Omega) = \mathrm{Re}\left[\mathrm{i} \sum_s H(t_s, t'_s, \mathbf{p}_s) a^*(t_s) \mathbf{d}(\mathbf{p}_s - e\mathbf{A}(t_s)/c) \right.$$
$$\left. \times\ \mathbf{E}(t'_s) \cdot \mathbf{d}(\mathbf{p}_s - e\mathbf{A}(t'_s)/c)\, a(t'_s) \mathrm{e}^{-iS_\Omega(\mathbf{p}_s, t_s, t'_s)/\hbar} \right] \quad (27)$$

with an additional Hessian factor $H(t_s, t'_s, \mathbf{p}_s)$ that accounts

ICFO
Institut de Ciències Fotòniques

(3) $\frac{\partial}{\partial t}$ | $\left(\bar{p} - \frac{e}{c}\bar{A}(t)\right)^2 / 2m + I_p = \hbar M \omega_L$ ← harmonic emission ($M = 2k+1$)

$\frac{\partial}{\partial t'}$ | $\left(\bar{p} - \frac{e}{c}\bar{A}(t')\right)^2 / 2m + I_p = 0$ tunneling

We calculate

$$p_{st} = eE\left[\frac{\cos\omega_L t - \cos(\omega_L(t-\tau))}{\omega_L^2 \tau}\right]$$

$\tau = t - t'$, return time

$$S_{st}(t,\tau) = (I_p + U_p)\tau + 2U_p\left(\frac{1 - \cos\omega_L\tau}{\omega_L^2\tau}\right) - \frac{U_p}{\omega_L} C(\tau) \cdot \cos\left(\omega_L\left(t - \frac{\tau}{2}\right)\right)$$

$$C(\tau) = \sin(\omega_L\tau) - 4\sin^2(\omega_L\tau/2)/\omega_L\tau$$

$$0 = \frac{\partial S_{st}}{\partial t} = \left(\bar{p}_{st} - \frac{e}{c}\bar{A}(t)\right)^2/2m - \left(\bar{p}_{st} - \frac{e}{c}\bar{A}(t-\tau)\right)^2/2m = \Delta E_{kin}(\tau) = (2k+1)\hbar\omega_L$$

$$\left(\bar{p}_{it} - \frac{e}{c}\bar{A}(t-\tau)\right)^2/2m + I_p = 0$$

18

$$2U_p C(\tau)\sin\left(2\omega_2\left(t-\frac{\tau}{2}\right)\right) = (2K+1)\hbar\omega_2$$

solution exists if

$$\left(\Delta E_{kin} \simeq\right)\ 2|C(\tau)| \geq (2K+1)\frac{\hbar\omega_2}{U_p}$$

3.

3.17

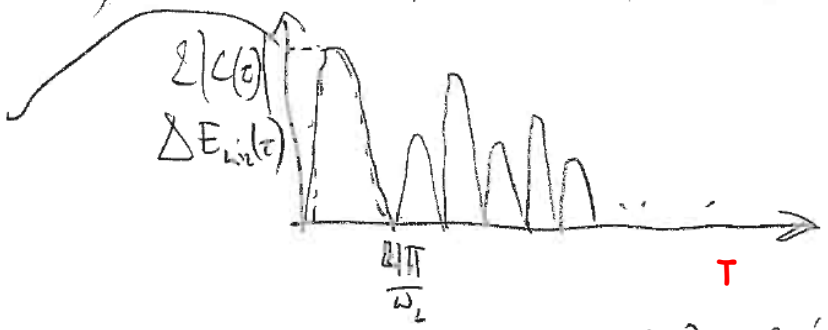

$$C(\tau) = 2\sin\frac{\tau}{2}\cos\frac{\tau}{2} - 4\sin\frac{\tau}{2}\sin\frac{\tau}{2}/\tau$$

$$\frac{\tau}{2} = M\pi \quad \text{or} \quad \cos\frac{\tau}{2} - \frac{2\sin\tau/2}{\tau} = 0$$

$$\tg x = x, \quad x = \frac{\tau}{2}$$

1.1.6 Attophysics

Why is it better than classical?

1. wave packet spreading
2. quantum interferences
3. quantum tunneling

How to generate

1. attosecond attoseconds pulse trains
2. single pulses from ultrashort
3. (ellipticity etc.

3.1 – Generalizations: ATI (direct tunelling)

$$b_0(\mathbf{p},t) = \frac{\mathrm{i}}{\hbar}\int_0^t \mathrm{d}t'\,\mathbf{E}(t')\cdot\mathbf{d}\left(\mathbf{p}-e\mathbf{A}(t')/c\right)a(t') \times \exp\left(-\mathrm{i}\int_{t'}^t \mathrm{d}\tilde{t}\left[\frac{1}{2m}\left(\mathbf{p}-e\mathbf{A}(\tilde{t})/c\right)^2 + I_p\right]/\hbar\right). \quad (16)$$

3.1 – Generalizations: ATI (re-scattering)

$$b_1(\mathbf{p},t) = \left(\frac{\mathrm{i}}{\hbar}\right)^2 \int_0^t \mathrm{d}t' \exp\left[-\mathrm{i}S(\mathbf{p},t,t')/\hbar\right] \mathbf{E}(t') \cdot \int_0^{t'} \mathrm{d}t'' \int \mathrm{d}^3\mathbf{p}' \mathbf{g}\left(\mathbf{p} - e\mathbf{A}(t')/c, \mathbf{p}' - e\mathbf{A}(t')/c\right) \times \mathbf{E}(t'') \cdot \mathbf{d}\left(\mathbf{p}' - e\mathbf{A}(t'')/c\right) a(t'') \exp\left[-\mathrm{i}S(\mathbf{p}',t',t'')/\hbar\right]. \quad (18)$$

ICFO
Institut de Ciències Fotòniques

3.2 – Generalizations: NSDI (EII)

$$d(\mathbf{p},\mathbf{p}',t) = \left(\frac{\mathrm{i}}{\hbar}\right)^2 \int_0^t \mathrm{d}t'' \int_0^{t''} \mathrm{d}t' \int \mathrm{d}^3\mathbf{p}'' \exp\left[\frac{\mathrm{i}}{\hbar} S_d(\mathbf{p},\mathbf{p}',t'',t)\right]$$
$$\times e\mathbf{E}(t'') \cdot \mathbf{g}(\mathbf{p} - e\mathbf{A}(t'')/c, \mathbf{p}' - e\mathbf{A}(t'')/c, \mathbf{p}'')$$
$$\times \exp\left[-\frac{\mathrm{i}}{\hbar} S_b(\mathbf{p}'',t',t'')\right] \mathbf{E}(t') \cdot \mathbf{d}(\mathbf{p}'' - e\mathbf{A}(t')/c)\, a(t'). \quad (62)$$

Rep. Prog. Phys. **82** (2019) 116001

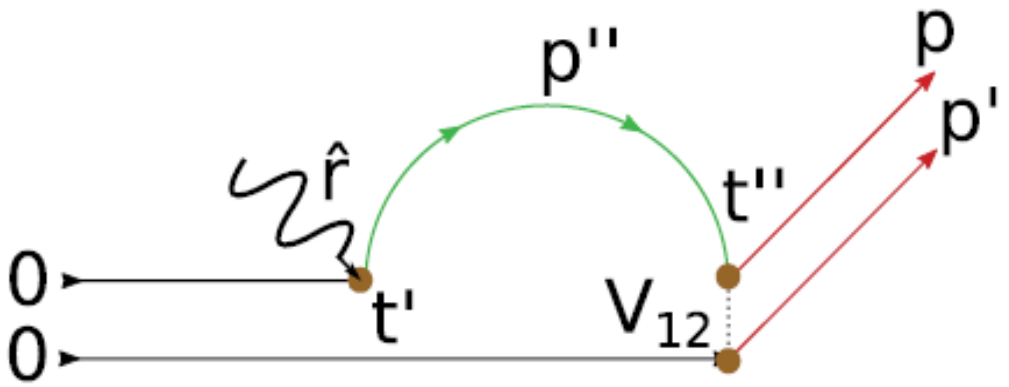

Figure 9. The complete EI process showing the two transitions. The two nodes marked at t' and t'' show the two transitions identified in the chain in equation (60).

ICFO
Institut de Ciències Fotòniques

3.3 – Generalizations: NSDI (RESI)

Rep. Prog. Phys. **82** (2019) 116001

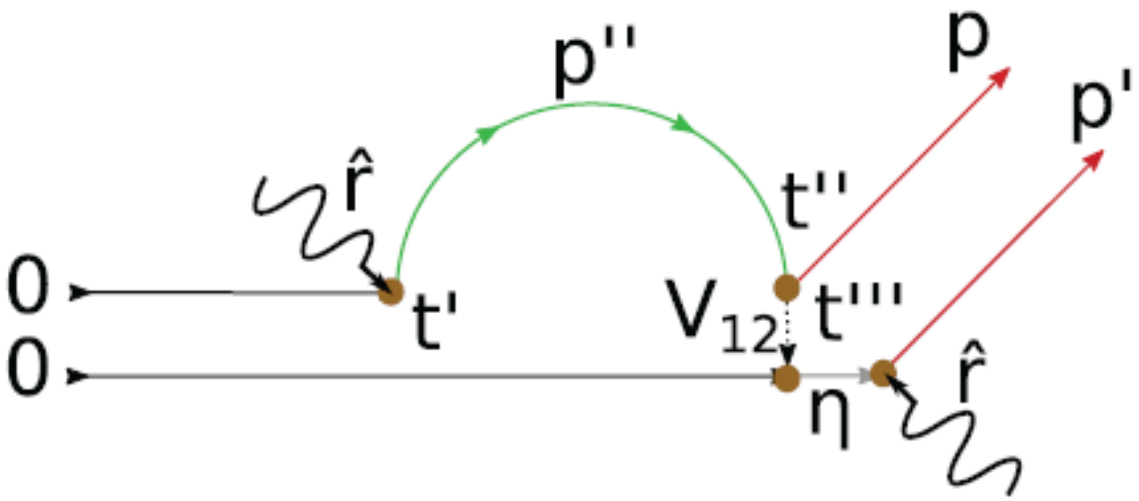

Figure 7. The complete RESI process showing all three transitions. The three nodes marked at the times t', t'' and t''' show the three transitions identified in the chain in equation (40).

3.3 – Generalizations: NSDI (RESI)

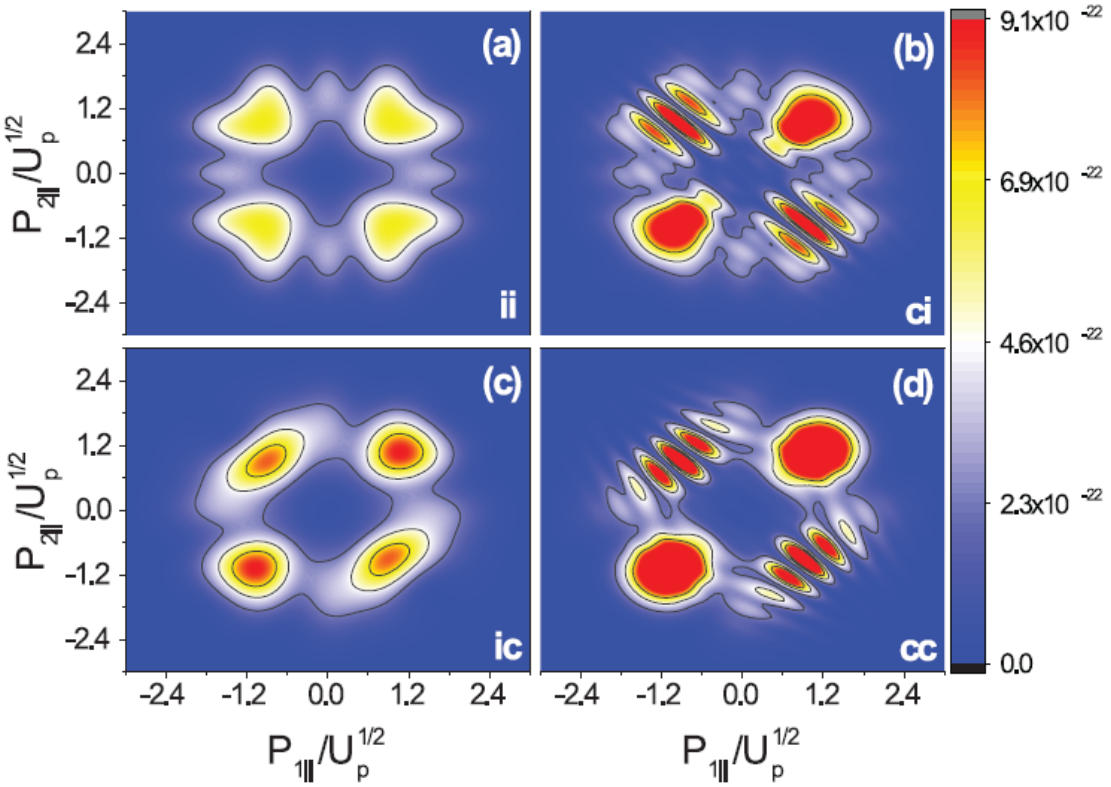

Figure 8. Momentum distribution of RESI for argon showing coherent and incoherent sums of pathways relating to different intermediate excited states and pathways related by symmetries. Whether the sum is coherent or incoherent (denoted c and i) is given in the bottom right for both the pathways relating to symmetries and excited states respectively. The ponderomotive energy is given by $U_p = 0.1$ a.u. ($I = 4.56 \times 10^{13}$ W cm^{-2}) corresponding to an angular frequency $\omega = 0.057$ a.u. or wavelength $\lambda = 800$ nm. Reprinted figure with permission from [186], Copyright (2015) by the American Physical Society.

3.3 – Generalizations: NSDI (RESI)

$$
\begin{aligned}
d(\mathbf{p},\mathbf{p}',t) = & \left(\frac{\mathrm{i}}{\hbar}\right)^3 \sum_{\eta\neq 0} \int_0^t \mathrm{d}t''' \int_0^{t'''} \mathrm{d}t'' \int_0^{t''} \mathrm{d}t' \int \mathrm{d}^3\mathbf{p}'' \\
& \times \exp\left[\frac{\mathrm{i}}{\hbar} S_d\left(\mathbf{p},\mathbf{p}',t''',t\right)\right] \times \mathbf{E}(t''') \cdot \Big(\tilde{\mathbf{g}}(\mathbf{p}' - e\mathbf{A}(t''')/c, \mathbf{p} - e\mathbf{A}(t''')/c, \eta) \\
& \times \exp\left[-\frac{\mathrm{i}}{\hbar} S_c\left(\mathbf{p},t'',t'''\right)\right] \times \mathbf{E}(t'') \cdot \mathbf{g}(\mathbf{p} - e\mathbf{A}(t'')/c, \mathbf{p}'' \times -e\mathbf{A}(t'')/c, \eta) \\
& \times \exp\left[-\frac{\mathrm{i}}{\hbar} S_b\left(\mathbf{p}'',t',t''\right)\right] \times \mathbf{E}(t') \cdot \mathbf{d}(\mathbf{p}'' - e\mathbf{A}(t')/c) a(t') + \{\mathbf{p}' \to \mathbf{p}\} \Big).
\end{aligned}
\tag{59}
$$

Rep. Prog. Phys. **82** (2019) 116001

$$J_{\mathrm{er}}^{(i)}(t) = -\mathrm{i}\sum_j \frac{\mathrm{d}}{\mathrm{d}t}\int_{t_0}^{t}\mathrm{d}t'\int_{\overline{\mathrm{BZ}}}\mathrm{d}^3\mathbf{K}\,|d_{cv}^{(i)}\left(\mathbf{K}-e\mathbf{A}(t)/c\right)| \times |d_{cv}^{(j)}\left(\mathbf{K}-e\mathbf{A}(t')/c\right)|E^{(j)}(t') \times \mathrm{e}^{-\mathrm{i}S(\mathbf{K},t,t')/\hbar-(t-t')/T_2+\mathrm{i}\left(\phi_{cv}^{(j)}(\mathbf{K},t)-\phi_{cv}^{(i)}(\mathbf{K},t)\right)} + \mathrm{c.c.}, \tag{102}$$

where $S(\mathbf{K},t,t')$ is the so called quasi-classical action for the electron–hole and is defined according to:

$$S(\mathbf{K},t,t') = \int_{t'}^{t}\Big[\varepsilon_g(\mathbf{K}-e\mathbf{A}(t'')/c) + e\mathbf{E}(t'')\cdot\boldsymbol{\xi}_g(\mathbf{K}-e\mathbf{A}(t'')/c) - \hbar\frac{\mathrm{d}}{\mathrm{d}t''}\phi_{cv}^{(j)}(\mathbf{K}-e\mathbf{A}(t'')/c)\Big]\mathrm{d}t''. \tag{103}$$

3.4 – Generalizations: Solids

PHYSICAL REVIEW B **102**, 134115 (2020)

Editors' Suggestion

Circular dichroism in higher-order harmonic generation: Heralding topological phases and transitions in Chern insulators

Alexis Chacón,[1,2,*] Dasol Kim,[2] Wei Zhu,[1] Shane P. Kelly,[1,3] Alexandre Dauphin,[4] Emilio Pisanty,[4] Andrew S. Maxwell,[4,5] Antonio Picón,[4,6] Marcelo F. Ciappina,[4,7,8,9] Dong Eon Kim,[2] Christopher Ticknor,[1] Avadh Saxena,[1] and Maciej Lewenstein[4,10]

[1]*Center for Nonlinear Studies and Theoretical Division, Los Alamos National Laboratory, Los Alamos, New Mexico 87545, USA*
[2]*Department of Physics and Center for Attosecond Science and Technology, POSTECH, 7 Pohang 37673, South Korea and Max Planck POSTECH/KOREA Research Initiative, Pohang, 37673, South Korea*
[3]*Physics and Astronomy Department, University of California Riverside, Riverside, California 92521, USA*
[4]*ICFO – Institut de Ciencies Fotoniques, The Barcelona Institute of Science and Technology, 08860 Castelldefels (Barcelona), Spain*
[5]*Department of Physics & Astronomy, University College London, Gower Street, London WC1E 6BT, United Kingdom*
[6]*Departamento de Química, Universidad Autónoma de Madrid, 28049 Madrid, Spain*
[7]*Institute of Physics of the ASCR, ELI-Beamlines project, Na Slovance 2, 182 21 Prague, Czech Republic*
[8]*Physics Program, Guangdong Technion – Israel Institute of Technology, Shantou, Guangdong 515063, China*
[9]*Technion – Israel Institute of Technology, Haifa 32000, Israel*
[10]*ICREA, Pg. Lluís Companys 23, 08010 Barcelona, Spain*

(Received 15 July 2020; accepted 2 September 2020; published 21 October 2020)

Topological materials are of interest to both fundamental science and advanced technologies because topological states are robust with respect to perturbations and dissipation. Experimental detection of topological invariants is thus in great demand but remains extremely challenging. Ultrafast laser-matter interactions, and in particular high-harmonic generation, meanwhile, were proposed several years ago as tools to explore the structural and dynamical properties of various matter targets. Here we show that the high-harmonic emission signal produced by a circularly polarized laser contains signatures of topological phases and transitions in the paradigmatic Haldane model. In addition to clear shifts of the overall emissivity and harmonic cutoff, the high-harmonic emission shows a unique circular dichroism, which exhibits clear changes in behavior at the topological phase boundary. Our findings pave the way to understand fundamental questions about the ultrafast electron-hole pair dynamics in topological materials via nonlinear high-harmonic generation spectroscopy.

DOI: 10.1103/PhysRevB.102.134115

3.4 – Generalizations: Solids

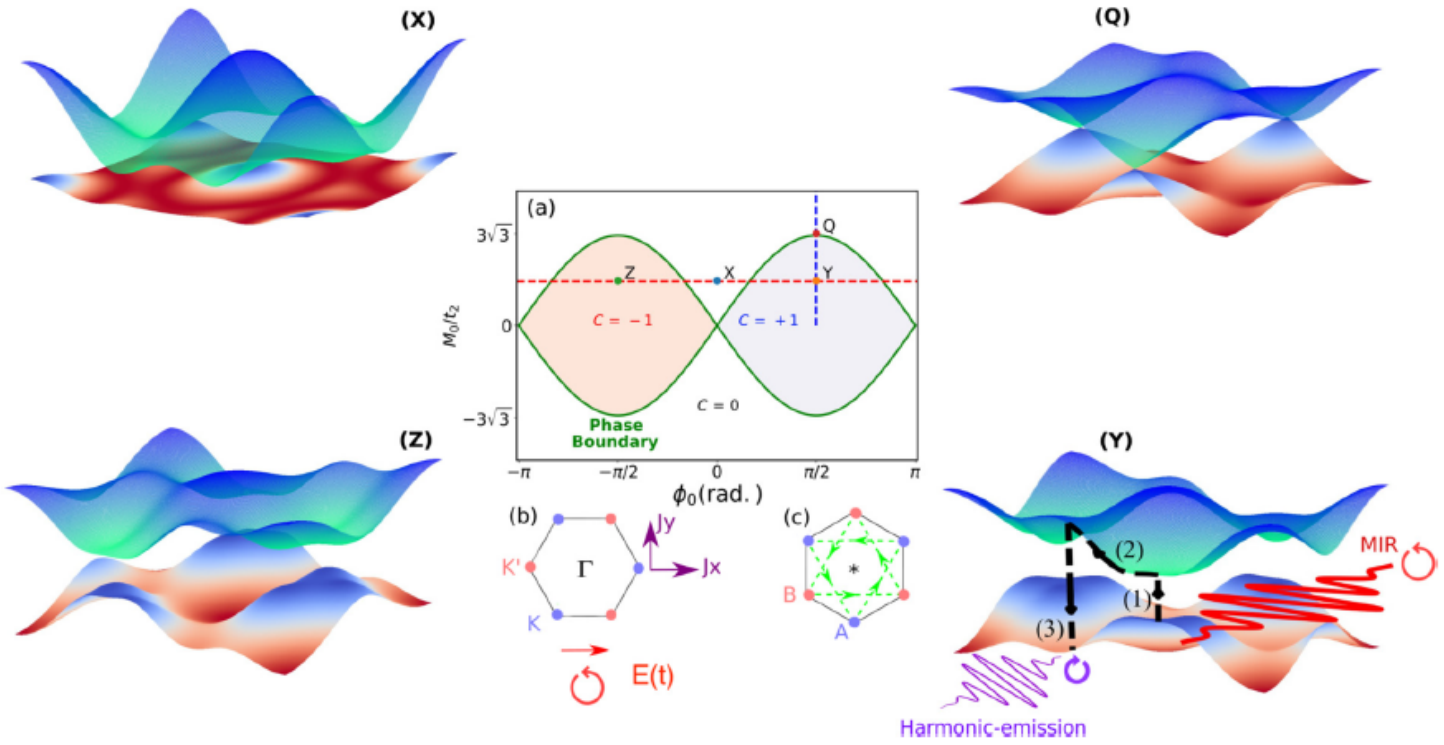

FIG. 1. Phase diagram and band structures of the Haldane model. (a) Phase diagram in the plane (ϕ_0, M_0/t_2), with the different phases labeled by their Chern number C; the green line shows the boundary of the topological phase transition. The band-structure diagrams correspond to the points X, Y, Z, and Q as marked in (a), with the point Q at the phase transition showing the gapless Dirac cone at the K point. (Y) and (Z) depict the band structure when the conduction-band topological invariants are $C = \pm 1$ at the phase points $\phi_0 = \pm\pi/2$ and $M_0 = 2.54t_2$. (Y) shows how the midinfrared laser-source oscillations (red-solid line) drive the topological material; this can be with both linear and circular polarizations. We also depict a physical cartoon of the electron-hole pair dynamics driven by a linearly polarized laser, i.e., creation, propagation, and annihilation or recombination by the black-dashed lines with arrows, and finally the subsequent harmonic emission (violet oscillations). The dashed lines in (a) indicate the cuts used for the parameter scans below. Panels (b) and (c) show the Brillouin zone and the real-space lattice of the Haldane model with the couplings in use.

3.4 – Generalizations: Solids

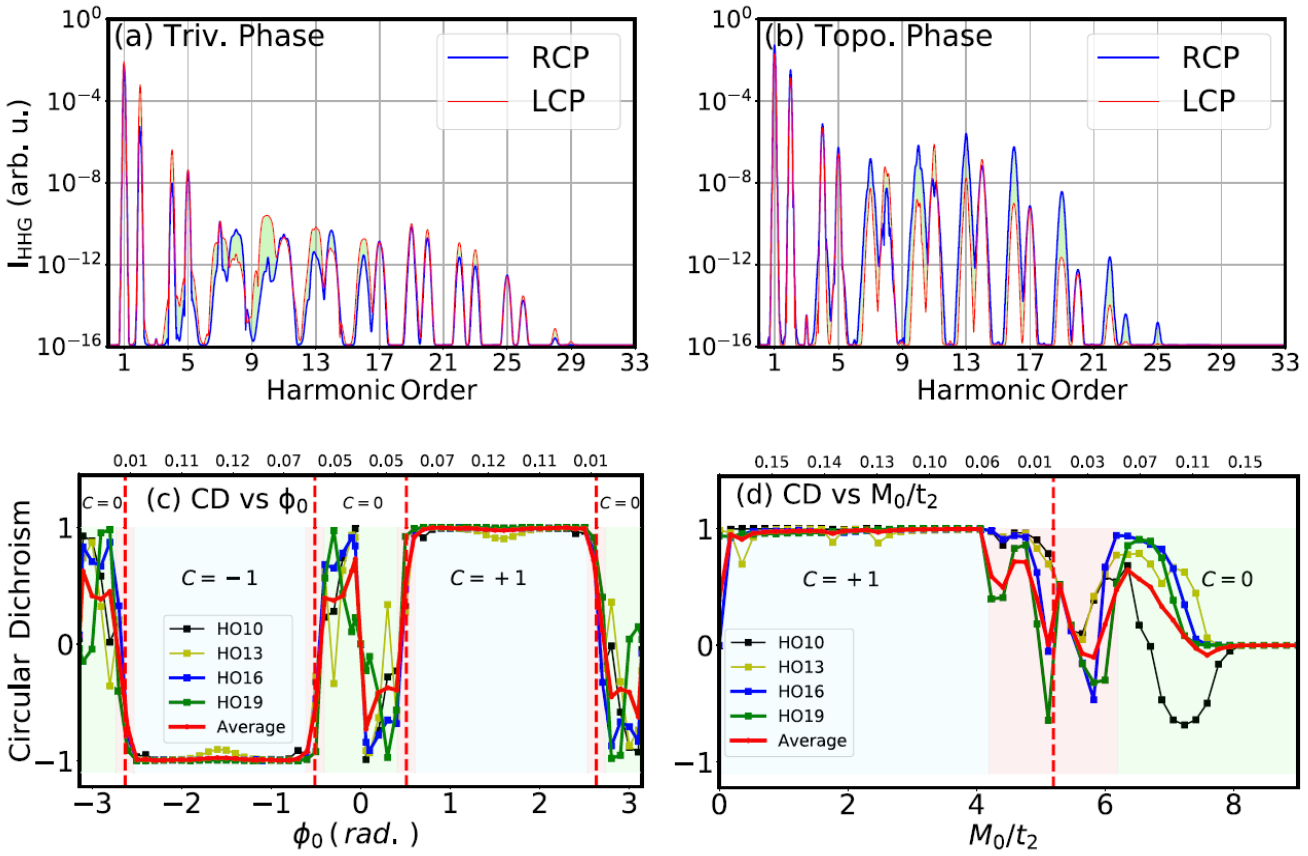

FIG. 5. Circular dichroism as a signature of topological phase transitions in HHG. (a), (b) Harmonic spectra of equal band-gap instances from the trivial and the topological phase, respectively, driven by right- and left-circularly polarized lasers, with the difference between the two emissions shaded in green. (We use the same parameters as in Fig. 3.) (c), (d) Circular dichroism (CD), as defined in Eq. (46), for the magnetic-flux and staggering potential parameter scans marked with dashed lines in Fig. 1, for the plateau harmonics. The top horizontal axes show the energy band gap E_g in atomic units (a.u.) as a function of ϕ_0 (c) and M_0/t_2 (d), respectively. The trivial and topological regions are shaded green and blue, with the critical region shaded red.

3.4 – Generalizations: Solids

IV. SEMICONDUCTOR BLOCH EQUATIONS

We introduce and examine the equations governing the microscopic time-dependent response of the solid due to the laser-matter interaction, the SBEs [66]. We follow the approach of Refs. [18,19], generalizing it to include the effects of possible nontrivial topology.

A. Semiconductor Bloch equations

If we write down the electronic-crystalline wave function in the form

$$|\Psi(t)\rangle = \sum_m \int_{\mathrm{BZ}} d\mathbf{k}\; a_m(\mathbf{k},t)|\Phi_{m,\mathbf{k}}\rangle, \tag{19}$$

the time evolution of the Bloch-space probability amplitudes $a_m(\mathbf{k},t)$, as determined by the Schrödinger equation, can be transformed into the form [62]

$$\mathrm{i}\dot{a}_m(\mathbf{k}',t) = \varepsilon_m(\mathbf{k}')a_m(\mathbf{k}',t) + \mathbf{E}(t)\cdot\sum_{m'}\int_{\mathrm{BZ}}\langle\Phi_{m,\mathbf{k}'}|\mathbf{x}|\Phi_{m',\mathbf{k}}\rangle a_{m'}(\mathbf{k}',t). \tag{20}$$

Here $\varepsilon_m(\mathbf{k})$ denotes the energy dispersion for the valence/conduction band $m = v,\ c$, and m' also ranges over both bands. We then compute the second and third terms on the right-hand side of the above equation by using Eq. (7), and we find

$$\dot{a}_m(\mathbf{k},t) = -\mathrm{i}[\varepsilon_m(\mathbf{k}) + \mathbf{E}(t)\cdot\boldsymbol{\xi}_m(\mathbf{k}) - \mathrm{i}\mathbf{E}(t)\cdot\nabla_{\mathbf{k}}]a_m(\mathbf{k},t) - \mathrm{i}\mathbf{E}(t)\cdot\sum_{m'\neq m}\mathbf{d}_{mm'}(\mathbf{k})\,a_{m'}(\mathbf{k},t). \tag{21}$$

This differential equation mixes time derivatives with the momentum gradient $\nabla_{\mathbf{k}}$, which also occurs for strong field approximation (SFA) treatment of atoms [13]. Thus, we apply the same transformation, shifting the momentum over time to $\mathbf{K} = \mathbf{k} - \mathbf{A}(t)$—the canonical crystal quasi-momentum, which is a constant of motion—giving rise to a shifted Brillouin zone, denoted $\overline{\mathrm{BZ}}$. More formally, by applying the substitution $a_m(\mathbf{k},t) = e^{\mathbf{A}(t)\cdot\nabla_{\mathbf{K}}}\, b_m(\mathbf{K},t)$, one finds that

$$\dot{b}_m(\mathbf{K},t) = -\mathrm{i}[\varepsilon_m(\mathbf{K}+\mathbf{A}(t)) + \mathbf{E}(t)\cdot\boldsymbol{\xi}_m(\mathbf{K}+\mathbf{A}(t))]b_m(\mathbf{K},t) - \mathrm{i}\mathbf{E}(t)\cdot\sum_{m'\neq m}\mathbf{d}_{mm'}(\mathbf{K}+\mathbf{A}(t))\,b_{m'}(\mathbf{K},t). \tag{22}$$

We then transform the transition amplitude b_m to the density matrix operator $\hat{\rho}$, i.e., the population $n_m = \rho_{mm}$ and coherence $\pi = \rho_{cv}$, given explicitly by $n_m(\mathbf{K},t) = b_m^*(\mathbf{K},t)b_m(\mathbf{K},t)$, and $\pi(\mathbf{K},t) = b_c(\mathbf{K},t)b_v^*(\mathbf{K},t)$. Thus, this leads to the SBEs, which describe the laser-electron interaction in the lattice [24] in terms of the band population and coherence:

$$\dot{n}_m(\mathbf{K},t) = \mathrm{i}(-1)^m\mathbf{E}(t)\cdot\mathbf{d}_{cv}^*(\mathbf{K}+\mathbf{A}(t))\,\pi(\mathbf{K},t) + \mathrm{c.c.}, \tag{23}$$

$$\dot{\pi}(\mathbf{K},t) = -\mathrm{i}\left[\varepsilon_g(\mathbf{K}+\mathbf{A}(t)) + \mathbf{E}(t)\cdot\boldsymbol{\xi}_g(\mathbf{K}+\mathbf{A}(t)) - \mathrm{i}\frac{1}{T_2}\right]\pi(\mathbf{K},t) - \mathrm{i}\mathbf{E}(t)\cdot\mathbf{d}_{cv}(\mathbf{K}+\mathbf{A}(t))\,w(\mathbf{K},t). \tag{24}$$

3.4 – Generalizations: Solids

ICFO Institut

B. Microscopic currents

The HHG spectra are obtained by Fourier analyzing microscopic charge currents induced by the driving laser pulse. Here we derive the total microscopic current $\mathbf{J}(t) = \mathbf{J}_{\rm ra}(t) + \mathbf{J}_{\rm er}(t)$, by focusing on its two components: the intraband $\mathbf{J}_{\rm ra}(t)$ and the interband $\mathbf{J}_{\rm er}(t)$ currents [18,19].

1. Interband current

We start by writing the interband current $\mathbf{J}_{\rm er}(t) = \frac{d}{dt}\mathbf{P}_{\rm er}(t)$ in terms of the polarization

$$\begin{aligned}\mathbf{P}_{\rm er}(t) &\equiv e\langle\Psi(t)|\mathbf{x}|\Psi(t)\rangle \\ &= e\int_{\rm BZ} d\mathbf{k}' \int_{\rm BZ} d\mathbf{k}\, a_c(\mathbf{k}',t)\, a_v^*(\mathbf{k},t) \\ &\quad\times \langle\Phi_{v,\mathbf{k}'}|\mathbf{x}|\Phi_{c,\mathbf{k}}\rangle + \text{c.c.}, \end{aligned} \tag{26}$$

where $e = -1$ a.u. is the electron charge. Next, using the identities above, the current simplifies to

$$\mathbf{J}_{\rm er}(t) = e\frac{d}{dt}\int_{\overline{\rm BZ}} \mathbf{d}_{cv}^*(\mathbf{K} + \mathbf{A}(t))\pi(\mathbf{K},t)\, d^2\mathbf{K} + \text{c.c.}, \tag{27}$$

indexed by the constant canonical crystal quasimomentum $\mathbf{K}$. This result coincides with the ones found by Vampa *et al.* in Ref. [67].

2. Intraband current

We write the intraband current, defined as $\mathbf{J}_{\rm ra}(t) = e\sum_m \langle\Psi(t)|\boldsymbol{v}_m|\Psi(t)\rangle$, in terms of the intraband velocity operator $\boldsymbol{v}_m = -\mathrm{i}\,[x_m, H_0] - \mathrm{i}\,[x_m, x_m\cdot\mathbf{E}(t)]$. We use the electromagnetic length gauge with the single-active-electron Hamiltonian and the dipole approximation of the laser-crystal system, i.e., $H(t) = H_0 + \mathbf{x}\cdot\mathbf{E}(t)$. For simplicity, our derivation is focused on the conduction band $m = c$ of the intraband current, which reads

$$\begin{aligned}\mathbf{J}_{\rm ra}(t) &= e\int d\mathbf{k}' \int d\mathbf{k}\, a_{c,\mathbf{k}'}^*(t) a_{c,\mathbf{k}}(t)\, \langle\Phi_{c,\mathbf{k}'}|x_c|\Phi_{c,\mathbf{k}}\rangle \varepsilon_c(\mathbf{k}) \\ &\quad + (c\to v) \\ &= e\int d\mathbf{k}'\, [n_c(\mathbf{k}',t)\,\mathbf{v}_c(\mathbf{k}') + n_v(\mathbf{k}',t)\,\mathbf{v}_v(\mathbf{k}')]. \end{aligned} \tag{28}$$

Here, $\mathbf{v}_c(\mathbf{k}) = \mathbf{v}_{{\rm gr},c}(\mathbf{k}) + \mathbf{v}_{a,c}(\mathbf{k})$ is written in terms of the group velocity $\mathbf{v}_{{\rm gr},c}(\mathbf{k}) = \nabla_{\mathbf{k}}\varepsilon_c(\mathbf{k})$, and the anomalous velocity $\mathbf{v}_{a,c}(\mathbf{k}) = -\mathbf{E}(t)\times\boldsymbol{\Omega}_c(\mathbf{k})$, where $\boldsymbol{\Omega}_m(\mathbf{k}) = \nabla_{\mathbf{k}}\times\boldsymbol{\xi}_m(\mathbf{k})$ is the Berry curvature. The anomalous-velocity term comes from considering that the intraband component $x_m^{(j)}$ of the position operator does not commute with $x_m^{(i)}$ component, with $i, j = x, y$ for 2D [62]. This intraband current also can be expressed on the shifted Brillouin zone $\overline{\rm BZ}$, as

$$\mathbf{J}_{\rm ra}(t) = e\sum_m \int_{\overline{\rm BZ}} \mathbf{v}_m(\mathbf{K} + \mathbf{A}(t))n_m(\mathbf{K},t)\, d^2\mathbf{K}. \tag{29}$$

3.4 – Generalizations: Solids

V. KELDYSH APPROXIMATION AND QUASICLASSICAL ANALYSIS

We may gain more insight into the physics of HHG by applying the so-called Keldysh approximation, as discussed for instance by Vampa *et al.* [67]. This approximation in a crystal solid reads $w(\mathbf{k},t) = n_v(\mathbf{k},t) - n_c(\mathbf{k},t) \approx 1$. Essentially, this means that the population transferred to the conduction band is very small compared to that remaining in the valence band. This approximation is very similar, but never equal, to the one used in the strong field approximation (SFA), developed originally for atoms and molecules [13–15]—we will thus term it SFA in the following. We focus on the discussion of

current,

$$J_{\mathrm{er}}^{(i)}(t) = -\mathrm{i}\sum_j \frac{d}{dt}\int_{t_0}^{t} dt' \int_{\mathrm{BZ}} d^2\mathbf{K}\, d_{cv}^{(i)}(\mathbf{K}+\mathbf{A}(t)) \times d_{cv}^{(j)}(\mathbf{K}+\mathbf{A}(t'))E^{(j)}(t') \times e^{-\mathrm{i}S(\mathbf{K},t,t')-(t-t')/T_2} + \mathrm{c.c.}, \quad (30)$$

where $S(\mathbf{K},t,t')$ is the so-called quasiclassical action for the electron-hole, which is defined as

$$S(\mathbf{K},t,t') = \int_{t'}^{t} [\varepsilon_g(\mathbf{K}+\mathbf{A}(t'')) + \mathbf{E}(t'')\cdot\boldsymbol{\xi}_g(\mathbf{K}+\mathbf{A}(t''))]dt''. \quad (31)$$

Here, $j = x, y$ indicates the component of the electric field and transition-dipole product which depends on the polarization of the driving laser.

This integral form of the interband current has a nice physical interpretation in terms of the electron-hole (e-h) pair:

(i) At time t', the e-h pair is excited by the driving laser from the valence band to the conduction band through the dipolar interaction $\mathbf{E}(t')\cdot\mathbf{d}_{cv}(\mathbf{K}+\mathbf{A}(t'))$ at the canonical crystal quasimomentum $\mathbf{K}$.

(ii) The e-h pair propagates in the conduction band and valence band, respectively, between t' and t, and modifies their trajectories and energies according to Eq. (37) below.

(iii) At time t, the electron has a probability to recombine (or annihilate) with the hole, at which point it emits its excess energy as a high energy-photon.

The expressions Eqs. (30) and (31) are the direct analogues of the Landau-Dykhne formula for HHG in atoms, derived in Ref. [15], following the idea of the simple man's model [14] (see also Ref. [13] for a recent review). Below we will analyze these expressions using the saddle-point approximation over crystal momentum to derive the effects of the Berry curvature on the relevant trajectories.






3.5 – Generalizations?: Strongly correlated materials

ICFO Institut de Ciències Fotòniques

High harmonic spectroscopy of quantum phase transitions in a high-T_c superconductor

Jordi Alcalà[1], Utso Bhattacharya[2,†], Jens Biegert[2,3,*], Marcelo Ciappina[4,5], Ugaitz Elu[2,†], Tobias Graß[2], Piotr T. Grochowski[2,6,7,8], Maciej Lewenstein[2,3], Anna Palau[1], Themistoklis P. H. Sidiropoulos[2], Tobias Steinle[2], and Igor Tyulnev[2]

[1]ICMAB-CSIC - Institut de Ciència de Materials de Barcelona, Campus UAB, 08193 Bellaterra, Spain
[2]ICFO - Institut de Ciencies Fotoniques, The Barcelona Institute of Science and Technology, 08860 Castelldefels (Barcelona), Spain
[3]ICREA, Pg. Lluís Companys 23, 08010 Barcelona, Spain
[4]Guangdong Technion - Israel Institute of Technology, Shantou, 515063 Guangdong, China
[5]Technion - Israel Institute of Technology, 32000 Haifa, Israel
[6]Center for Theoretical Physics, Polish Academy of Sciences, Aleja Lotników 32/46, 02-668 Warsaw, Poland
[7]Institute for Quantum Optics and Quantum Information, Austrian Academy of Sciences, A-6020 Innsbruck, Austria
[8]Institute for Theoretical Physics, University of Innsbruck, A-6020 Innsbruck, Austria
[†]These authors contributed equally
[*]Corresponding author: jens.biegert@icfo.eu

January 25, 2022

arXiv:2201.09515v1 [cond-mat.supr-con] 24 Jan 2022

In print in PNAS

3.5 – Generalizations?: Strongly correlated materials

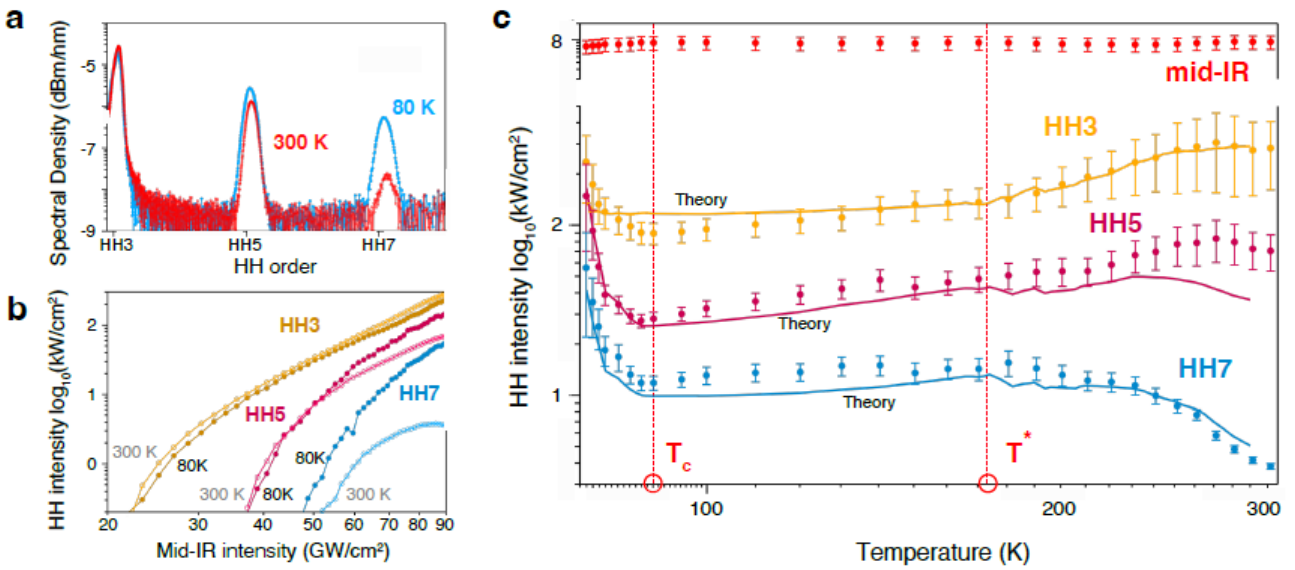

Figure 2: **High harmonic spectroscopy of YBCO:** (a) Harmonic spectra showing odd orders HH3, HH5 and HH7 for room temperature (red) and at $T_c = 90K$ (blue) for a mid-IR field strength of 0.083 V/Å. Visible is already a blueshift of room-temperature harmonics with increasing harmonic order and relative to the harmonics measured at T_c. We observe a dramatic increase of HH7 amplitude upon cooling into the SC phase. (b) Shown is the scaling of harmonic order with mid-IR peak-intensity for measurements at room temperature and at T_c. Dark colours show data for the SC phase whereas light colours indicate data at room temperature. (c) Shown is the reflected mid-IR field together with harmonics HH3, HH5 and HH7 as a function of temperature. These measurements are taken for a mid-IR field strength of 0.083 V/Å. Results from the strong-field quasi-Hubbard model are overlaid as solid lines. We observe a dramatic increase of HH7 amplitude upon cooling into the SC phase at 88 K. All harmonic orders show a clear turning point at the critical temperature T_c and an exponential increase in amplitude. More subtle, but still clearly discernible is another critical point T^* at 173 K, marking the transition from strange metal to the pseudogap phase. The functional behaviour is reproduced by the model.

3.5 – Generalizations?: Strongly correlated materials

ICFO Institut de Ciències Fotòniques

Theoretical model. The theoretical description is based on a Hubbard-like two-band model in the BCS limit, whose time-dependent Hamiltonian reads

$$H(t) = \sum_{k,\lambda,\sigma} \varepsilon_{k\lambda} c^{\dagger}_{k\sigma\lambda}(t) c_{k\sigma\lambda}(t) + \sum_{k} [\Delta_k(t) c^{\dagger}_{k\uparrow \mathrm{L}}(t) c^{\dagger}_{-k\downarrow \mathrm{L}}(t) + \mathrm{h.c.}]$$
$$- E(t) \sum_{k,\lambda,\lambda',\sigma} [c^{\dagger}_{k\sigma\lambda}(t) D_{\lambda\lambda'}(k) c_{k\sigma\lambda'}(t)]. \quad [1]$$

Here, $\lambda \in \{\mathrm{L}, \mathrm{U}\}$ is the band index for the lower and upper band, $\sigma \in \{\downarrow, \uparrow\}$ is the spin index, and k is the index for pseudomomentum. The operators $c_{k\sigma\lambda}(t)$ and $c^{\dagger}_{k\sigma\lambda}(t)$ are the corresponding time-dependent annihilation and creation operators in the Heisenberg frame. The band energies are given by $\varepsilon_{k\mathrm{U}} = E_g + E_{\mathrm{U}}(k) - \mu$ and $\varepsilon_{k\mathrm{L}} = E_{\mathrm{L}}(k) - \mu$, where μ is the chemical potential, determined self-consistently. The renormalized band structure along the main symmetry direction is obtained from DFT, and parametrized by the functions $E_\lambda(k)$, and a direct energy gap $E_g = 0.0317$ a.u. at the band edge.

The second term in Eq. (1) is the pairing term, proportional to the time-dependent superconducting gap $\Delta_k(t)$. This term is obtained from an attractive d-wave interaction $U_k = U[\cos(k_x a) - \cos(k_y a)]$ of strength U, and the gap parameter must fulfill the BCS self-consistency condition $\Delta_k(t) = -U_k \left[\sum_{k'} U_{k'} \langle c_{-k'\downarrow \mathrm{L}}(t) c_{k'\uparrow \mathrm{L}}(t)\rangle\right]$.

The last term in Eq. (1) describes the coupling to the light field, with an electric field pulse $E(t) = E_0 \sin^2(\omega_0 t/2n_{\mathrm{cyc}}) \sin(\omega_0 t)$ of amplitude $E_0 = 0.004$ in atomic units (a.u.), center frequency $\omega_0 = 0.01425$ a.u., $n_{\mathrm{cyc}} = 8$ cycles. These values are compatible with the experimental estimated parameters of the laser pulse. The optical coupling is proportional to the covariant derivative (1), $-iD_{\lambda\lambda'}(k) = \left[\delta_{\lambda\lambda'}\partial_k - id_{\lambda\lambda'(k)}\right]$, with $d_{\lambda\lambda'}(k)$ describing the interband dipole moment, or, for $\lambda = \lambda'$, the Berry connection of the respective band, which is zero in our system. For the dipole moment we have used d_{UL}=14 a.u. in our numerical evaluations.

electron-phonon interactions and disorder, we include in these equations non-unitary scattering processes with phenomenological scattering times τ_1 and τ_2:

$$i\partial_t \langle O(t)\rangle = -\langle [H(t), O(t)]\rangle - i\frac{\langle O(t)\rangle}{\tau_{1/2}}. \quad [2]$$

τ_1 is used when $O(t)$ represents a population, while τ_2 when $O(t)$ describes a correlation. The scattering times τ_1 and τ_2 and their temperature-dependence are obtained by fitting theoretical results to the experimental data, see main text Fig. 4.

3.5 – Generalizations?: Strongly correlated materials

Conclusions

ICFO Institut de Ciències Fotòniques

Conclusions?

Enjoy physics and beyond!!!

*iCrea INSTITUCIÓ CATALANA DE RECERCA I ESTUDIS AVANÇATS

Outline - Part II: Toward QED of Super-Intense Laser-Matter Physics

Maciej Lewenstein et al. Generation of optical Schrödinger cat states in intense laser matter interactions (Nature Phys. 17, 1104–1108, (2021),

4. General introduction: QED of Super-Intense Laser-Matter Physics
   - 4.1 TDSE
   - 4.2 Unitaries

5. Conditioning (on example of HHG)
   - 1.1 Final equation conditioned on the ground state
   - 1.2 Final state of the EM field
   - 1.3 Final conditioned state

6. Generalizations: Conditioning on
   - 3.1 ATI (direct tunneling, re-scattering)
   - 3.2 NSDI – Electron Impact Ionization (EII)
   - 3.3 NSDI – Resonant Excitation Subsequent Ionization (RESI)
   - 3.4 Solids

ICFO
Institut de Ciències Fotòniques

nature physics

LETTERS

https://doi.org/10.1038/s41567-021-01317-w

Check for updates

Generation of optical Schrödinger cat states in intense laser–matter interactions

M. Lewenstein[1,2] ✉, M. F. Ciappina[1,3,4,5], E. Pisanty[1,6], J. Rivera-Dean[1], P. Stammer[1,6], Th. Lamprou[7,8] and P. Tzallas[7,8,9] ✉

The physics of intense laser–matter interactions[1,2] is described by treating the light pulses classically, anticipating no need to access optical measurements beyond the classical limit. However, the quantum nature of the electromagnetic fields is always present[3]. Here we demonstrate that intense laser–atom interactions may lead to the generation of highly non-classical light states. This was achieved by using the process of high-harmonic generation in atoms[4,5], in which the photons of a driving laser pulse of infrared frequency are upconverted into photons of higher frequencies in the extreme ultraviolet spectral range. The quantum state of the fundamental mode after the interaction, when conditioned on the high-harmonic generation, is a so-called Schrödinger cat state, which corresponds to a superposition of two distinct coherent states: the initial state of the laser and the coherent state reduced in amplitude that results from the interaction with atoms. The results open the path for investigations towards the control of the non-classical states, exploiting conditioning approaches on physical processes relevant to high-harmonic generation.

and Schrödinger 'cat' states, and so on)[13–17], which are at the core of quantum technology[18–20].

To unmask the quantum nature of light in strongly laser-driven interactions and show its impact on the aforementioned directions, we have used the HHG process in atoms[4,5], which is one of the most fundamental processes in strong-laser-field physics. The understanding of the HHG process was boosted from the formulation of the semiclassical three-step model[12]. In this approach, HHG from a single atom/molecule/solid is initiated by an electron's tunnelling to the continuum, its subsequent acceleration in the intense laser field and finally its recombination to the ground state of the target. To provide a fully quantized description of the HHG process, we have to rigorously answer the following questions. (1) What is the quantum depletion of the coherent state of the fundamental laser mode? (2) What is the quantum state of the generated harmonics? Although several groups have attempted to study this problem theoretically[21–25] and experimentally[26,27], none of these efforts have provided a rigorous answer to the above questions. Here we show that if the initial state of a system of N atoms in their ground state

4. QED of Super-Intense Laser-Matter Physics

4.1 General introduction: TDSE

$$i\hbar \frac{\partial}{\partial t} \left|\bar{\Psi}(t)\right\rangle = \hat{H} \left|\bar{\Psi}(t)\right\rangle,$$

where

where the Hamiltonian, $\hat{H}$, describes the laser-target system in the single-active-electron (SAE) approximation, and is the sum of three terms, that is, $\hat{H} = \hat{H}_0 + \hat{U} + \hat{H}_f$, where $\hat{H}_0 = \frac{\hat{\mathbf{P}}^2}{2m} + V(\hat{\mathbf{r}})$ is the laser-free Hamiltonian of the atomic or molecular system with $V(\hat{\mathbf{r}})$ being the effective SAE atomic or molecular potential, m is the electron mass; $\hat{U} = -e\hat{\mathbf{E}} \cdot \hat{\mathbf{r}}$ is the dipole coupling, which describes the interaction of the atomic or molecular system with the laser radiation, written in the length gauge and under the dipole approximation; and, finally, $H_f = \int d\omega\, \hbar\omega \hat{a}^\dagger_\omega \hat{a}_\omega$ is the electromagnetic (EM) field Hamiltonian containing all the frequency modes.

$$\hat{H}_f = \hbar\omega\hat{a}^\dagger\hat{a} + \sum_q^{\text{cutoff}} \hbar\omega q\hat{b}_q^\dagger\hat{b}_q,$$

electric field operator as

$$\hat{\mathrm{E}} = -\mathrm{i}\hbar\mathrm{g}(\omega_\mathrm{L})f(t)\left[(\hat{a}^\dagger - \hat{a}) + \sum_3^{\text{cutoff}} \sqrt{q}(\hat{b}_q^\dagger - \hat{b}_q)\right]. \quad (7)$$

In equation (7), the dimensionless function $0 \leq f(t) \leq 1$ describes the envelope of the laser pulse normalized to one at maximum. We denote the effective coefficient entering into the expansion of the electric field into the modes by $\mathrm{g}(\omega) \propto \sqrt{\omega/V_{\text{eff}}}$, where V_{eff} is the effective quantization volume[33,34]. $e\mathrm{g}(\omega)$ encodes information about the polarization of the modes, has dimension $[\mathrm{m}^{-1}\,\mathrm{s}^{-1}]$, and for the typical frequencies used in strong-field physics is very small, on the order of 10^{-8} in a.u.

Equation (5) needs to be solved starting from the initial condition $|\tilde{\Psi}(0)\rangle = |g, \alpha_L, \Omega_H\rangle$, that is for the electron initially being in its ground state $|g\rangle$, the laser in a coherent state $|\alpha_L\rangle$ and the harmonics in the vacuum state $|\Omega_H\rangle$. To this aim, we write $|\tilde{\Psi}(t)\rangle = \exp[-i\hat{H}_f t/\hbar] D(\alpha_L) |\Psi(t)\rangle$, where $D(\alpha_L)$ is the Glauber's shift operator creating a coherent state $|\alpha_L\rangle$ from the vacuum of the laser mode, $|\Omega_L\rangle$. The second unitary operator transforms to the interaction picture with respect to the EM field. With these transformations, the initial state of the system is now described by $|\Psi(0)\rangle = |g, \Omega_L, \Omega_H\rangle$ and the electric field part of the Hamiltonian shown in equation (5) becomes time dependent and gains an extra factor describing the behaviour of the 'classical' field, that is, the mean value $\langle\alpha_L|\hat{E}(t)|\alpha_L\rangle$. More explicitly, our Schrödinger equation now reads

$$i\hbar\frac{\partial}{\partial t}|\Psi(t)\rangle = \left[\hat{H}_{sc} - e\hat{E}_Q(t)\cdot\hat{\mathbf{r}}\right]|\Psi(t)\rangle, \tag{8}$$

where $\hat{H}_{sc}(t) = \hat{H}_0 - eE_L(t)\cdot\hat{\mathbf{r}}$ and $E_L(t) = -i\hbar|\mathbf{g}(\omega_L)|f(t)[\alpha_L^* e^{i\omega_l t} - \alpha_L e^{-i\omega_l t}]$, the 'classical' electric field of the laser pulse. The quantum correction is

$$\hat{E}_Q(t) = -i\hbar\mathbf{g}(\omega_L)f(t)\left[\hat{a}^\dagger e^{i\omega_L t} - \hat{a}e^{-i\omega_L t} + \sum_{q=3}^{\text{cutoff}}\sqrt{q}[\hat{b}_q^\dagger e^{iq\omega_L t} - \hat{b}_q e^{-iq\omega_L t}]\right]. \tag{9}$$

4.2 General introduction: Unitaries

The next step is to go to the interaction picture with respect to $\hat{H}_{sc}(t)$, something that we achieve with the following transformation

$$|\Psi(t)\rangle = \mathcal{T} \exp\left[-i \int_0^t \hat{H}_{sc}(t')dt'/\hbar\right] |\psi(t)\rangle, \tag{10}$$

where $\mathcal{T}$ denotes the time-ordered product. Then we obtain:

$$i\hbar \frac{\partial}{\partial t} |\psi(t)\rangle = -e\hat{\mathbf{E}}_Q(t) \cdot \hat{\mathbf{r}}_H(t) |\psi(t)\rangle. \tag{11}$$

The transformation depicted in equation (10) does not alter the initial condition for the system, but introduces in our Schrödinger equation the dynamics

$$\hat{1} = |y\rangle\langle y| + \int d_2 v\, |v\rangle\langle v|$$

5. Conditioning on HHG

5.1 Conditioning on the ground state

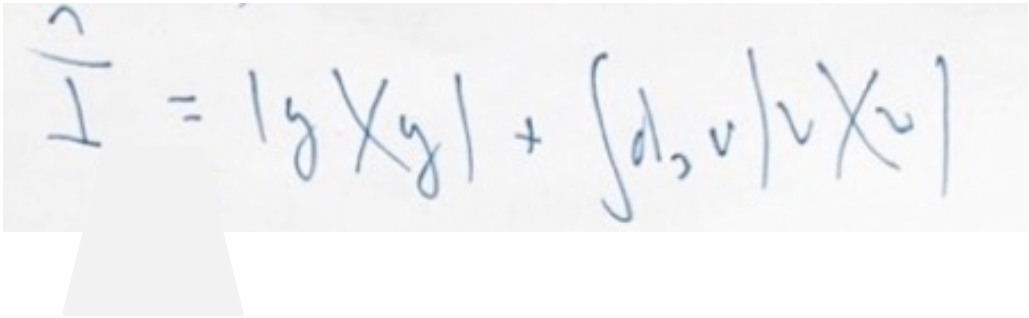

Therefore, it makes sense to condition equation (11) on the ground state, that is to consider $|\phi(t)\rangle = \langle g|\psi(t)\rangle$, which fulfills equation (1), that is

$$i\hbar\frac{\partial}{\partial t}|\phi(t)\rangle = -\hat{\mathbf{E}}_{\mathrm{Q}}(t)\cdot\langle\hat{\mathbf{d}}_{\mathrm{H}}(t)\rangle\,|\phi(t)\rangle\,, \tag{12}$$

where $\hat{\mathbf{E}}_{\mathrm{Q}}(t)$ is the quantum fluctuating part of the laser fields described in equation (9), and $\langle\hat{\mathbf{d}}_{\mathrm{H}}(t)\rangle$ is the quantum averaged time-dependent dipole moment over the ground state, that is, $\langle g|e\hat{\mathbf{r}}_{\mathrm{H}}(t)|g\rangle$, that can be efficiently calculated solving the TDSE, or even easier using the strong-field approximation[7,12]. Also, the effective Hamiltonian $\hat{H}_{\mathrm{Q}}(t) = -\hat{\mathbf{E}}_{\mathrm{Q}}(t)\cdot\langle\hat{\mathbf{d}}_{\mathrm{H}}(t)\rangle$ is a linear form of photon creation and annihilation operators. Thus, the unitary evolution operator is an exponent of a linear form of creation and annihilation operators, and thus when acting on coherent states, it will shift them. One can obviously calculate exactly the evolution

5.2 Final state of the EM field

$$i\hbar\frac{\partial}{\partial t}|\phi(t)\rangle = -\hat{\mathbf{E}}_{\mathrm{Q}}(t)\cdot\langle\hat{\mathbf{d}}_{\mathrm{H}}(t)\rangle\,|\phi(t)\rangle\,. \qquad (1)$$

tion[7,12]. The solution is (Methods):

$$|\phi(t)\rangle = \left|(\alpha_{\mathrm{L}}+\delta\alpha_{\mathrm{L}})\mathrm{e}^{-\mathrm{i}\omega_{\mathrm{L}}t}, \beta_3\mathrm{e}^{-3\mathrm{i}\omega_{\mathrm{L}}t}, \ldots, \beta_q\mathrm{e}^{-q\mathrm{i}\omega_{\mathrm{L}}t}, \ldots\right\rangle, \qquad (2)$$

where $\delta\alpha_{\mathrm{L}} = -\mathrm{i}\mathbf{g}(\omega_{\mathrm{L}})\cdot\mathbf{d}_{\omega_{\mathrm{L}}}$, $\beta_q = -\mathrm{i}\mathbf{g}(\omega_{\mathrm{L}})\sqrt{q}\cdot\mathbf{d}_{q\omega_{\mathrm{L}}}$, ω_{L} is the frequency of the fundamental laser field, and $\mathbf{g}(\omega_{\mathrm{L}})$ is the effective coefficient entering into the expansion of the electric field into the quantized modes (Methods). Here $\mathbf{d}_\omega = \int_0^T f(t)\mathrm{e}^{\mathrm{i}\omega t}\langle\hat{\mathbf{d}}_{\mathrm{H}}(t)\rangle$ is a Fourier transform of the time averaged semiclassical dipole moment (Methods) weighted by the pulse envelope $f(t)$. Assuming

that N atoms contribute to HHG coherently in a phase-matched way, we obtain that the final state of the fundamental and harmonic fields, after the pulse being coherent, is $|\alpha_L + \delta\alpha_L\rangle$ and $|\beta_q\rangle$ (Fig. 1) respectively, with

$$\delta\alpha_L = -iNg(\omega_L) \cdot \mathbf{d}_{\omega_L}, \tag{3}$$

$$\beta_q = -iNg(\omega_L)\sqrt{q} \cdot \mathbf{d}_{q\omega_L}. \tag{4}$$

$$|\phi(t)\rangle = \left|(\alpha_L + \delta\alpha_L)e^{-i\omega_L t}, \beta_3 e^{-3i\omega_L t}, \ldots, \beta_q e^{-qi\omega_L t}, \ldots\right\rangle, \tag{2}$$

5.3 Final conditioned state

ICFO Institut de Ciències Fotòniques

nature physics

LETTERS

https://doi.org/10.1038/s41567-021-01317-w

Check for updates

Generation of optical Schrödinger cat states in intense laser–matter interactions

M. Lewenstein[1,2] ✉, M. F. Ciappina[1,3,4,5], E. Pisanty[1,6], J. Rivera-Dean[1], P. Stammer[1,6], Th. Lamprou[7,8] and P. Tzallas[7,8,9] ✉

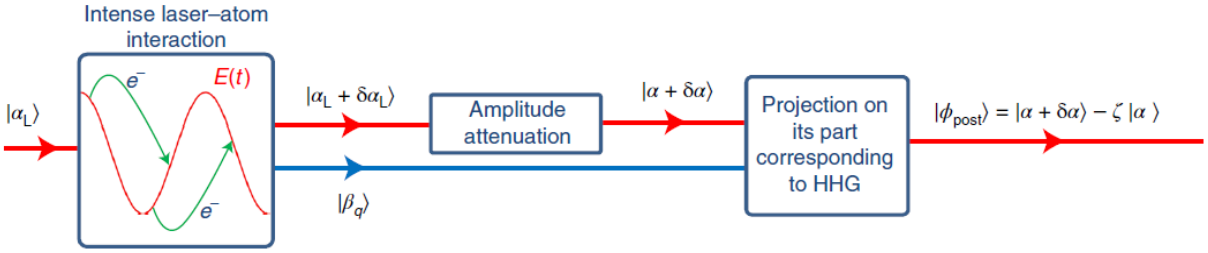

Fig. 1 | Schematic representation of the generation of optical 'cat' states. The coherent laser state $|\alpha_L\rangle$ (thick red lines) interacts with atoms and in consequence high harmonics (thick blue lines) are generated. The inset shows an intuitive picture of the electron recollision process that leads to HHG. The oscillating laser field $E(t)$ is depicted with thin red curve and the electron paths with thin green curves. After the interaction, the harmonic modes are coherent $|\beta_q\rangle$ and the fundamental is an amplitude-shifted coherent state $|\alpha_L + \delta\alpha_L\rangle$. This state after an amplitude attenuation ($|\alpha + \delta\alpha\rangle$), is projected on its part corresponding to HHG and becomes a Schrödinger 'cat' state $|\phi_{post}\rangle$ with $\zeta = \langle\alpha|\alpha + \delta\alpha\rangle$.

Quantum state characterization

Xenon gas jet OFF

coherent state

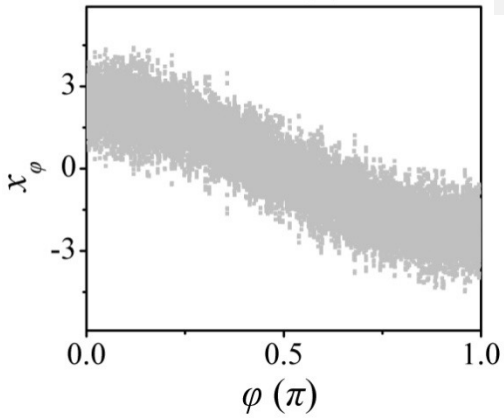

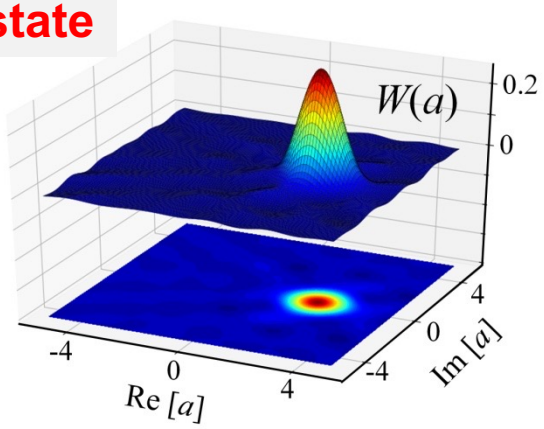

Xenon gas jet ON

“cat” state

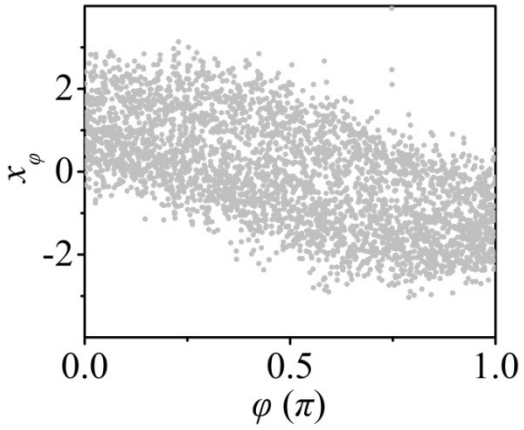

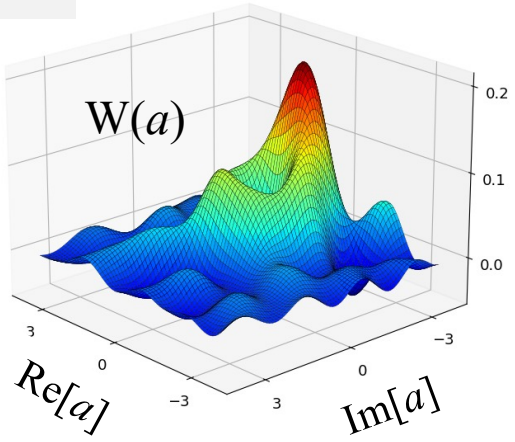

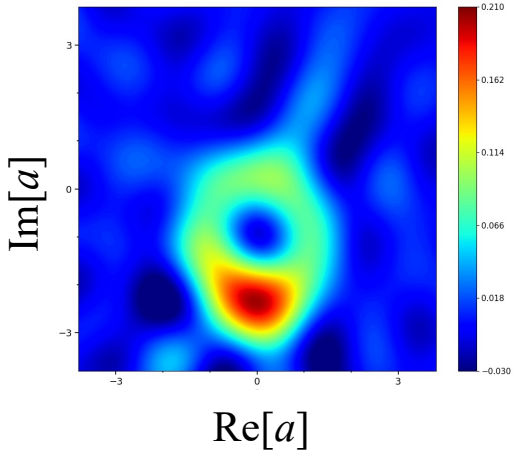

M. Lewenstein *et. al.*, arXiv/2008.10221 (2020), Nature Phys.17, 1104{1108 (2021).

FORTH
INSTITUTE OF ELECTRONIC STRUCTURE AND LASER

ICFO

Quantum state characterization

LETTERS NATURE PHYSICS

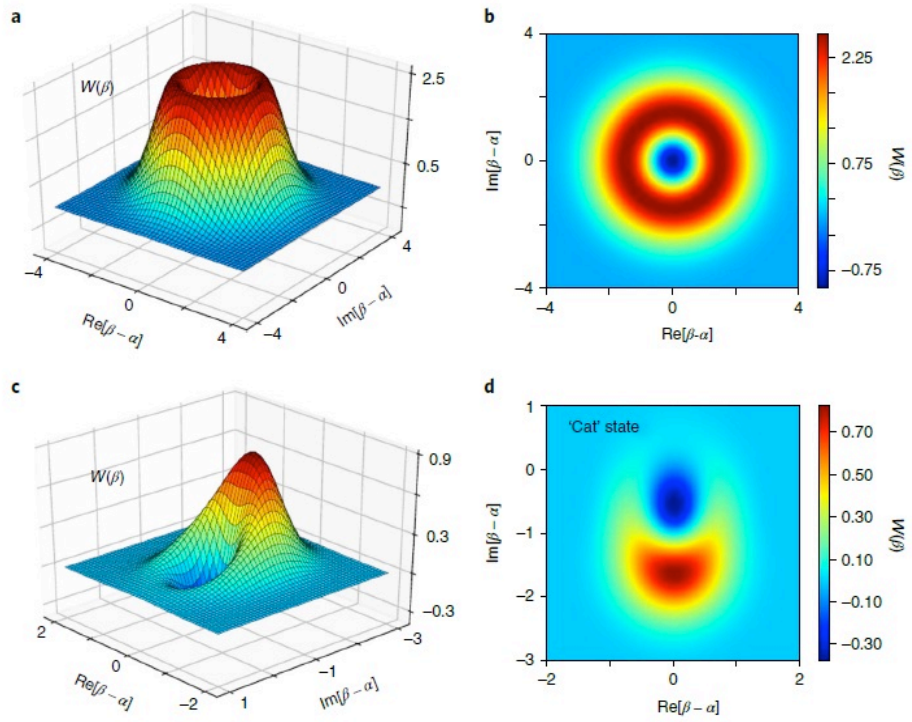

Fig. 2 | Calculated Wigner functions of a Schrödinger 'kitten' and a 'cat' state. The Wigner functions $W(\beta)$ are plotted according to the terminology of ref. [29]. β is a variable such that $\mathrm{Re}[\beta-\alpha]\equiv x$ and $\mathrm{Im}[\beta-\alpha]\equiv p$. x and p are the values of the quadrature field operators $\hat{x}=(\hat{a}+\hat{a}^{\dagger})/\sqrt{2}$ and $\hat{p}=(\hat{a}-\hat{a}^{\dagger})/i\sqrt{2}$. $\delta\alpha$ represents the amplitude shift of the initial coherent state $|\alpha\rangle$ and $\zeta=\langle\alpha|\alpha+\delta\alpha\rangle$ reflects the coupling between the initial coherent state and the shifted one $|\alpha+\delta\alpha\rangle$. **a**, Wigner function of a Schrödinger 'kitten' state, corresponding to a coherently shifted first Fock state for small $\delta\alpha$ where $|\zeta|\approx 1$. **b**, Projection of $W(\beta)$ shown in **a** on the $(\mathrm{Re}[\beta-\alpha],\mathrm{Im}[\beta-\alpha])$ plane. **c**, Wigner function of a genuine Schrödinger 'cat' state for $|\delta\alpha|=1.5$ (comparable to $|\alpha|=2$) where $|\zeta|\approx 0.32$. The Wigner depicts a ring structure with a maximum $W_{\mathrm{max}}\approx 0.8$ at $(x,p)\approx(0,-1.7)$ and a negative minimum $W_{\mathrm{min}}\approx -0.3$ at $(x,p)\approx(0,-0.7)$. The contrast $C=2(W_{\mathrm{max}}-W_{\mathrm{min}})/(W_{\mathrm{max}}+W_{\mathrm{min}})\approx 4.4$. It is noted that the exact shape of the Wigner function depends on the parameter ζ. Here we have used a ζ that provides a function reasonably close to the experimental results. **d**, Projection of $W(\beta)$ shown in **c** on the $(\mathrm{Re}[\beta-\alpha],\mathrm{Im}[\beta-\alpha])$ plane.

M. Lewenstein *et. al.*, arXiv/2008.10221 (2020), Nature Phys.17, 1104{1108 (2021).

FORTH
INSTITUTE OF ELECTRONIC STRUCTURE AND LASER

ICFO

Quantum state characterization

NATURE PHYSICS LETTERS

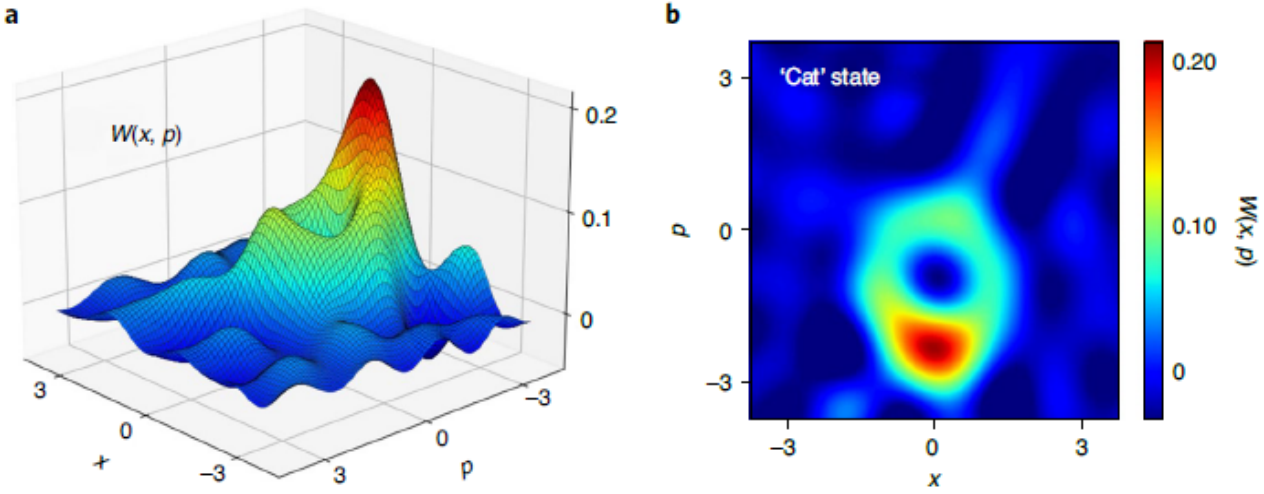

Fig. 4 | Measurement of the Wigner function of the genuine Schrödinger 'cat' state. a, Measured Wigner function $W(x,p)$ of the IR field (with $\langle n\rangle \approx 1.98 \pm 0.04$) when the HHG process and the conditioning to the HHG, were switched on (that is, xenon gas jet and QS switched on). x and p are the values of the quadrature field operators $\hat{x} = (\hat{a} + \hat{a}^{\dagger})/\sqrt{2}$ and $\hat{p} = (\hat{a} - \hat{a}^{\dagger})/i\sqrt{2}$. The error of the amplitude of $W(x,p)$ is ± 0.002. In agreement with the theoretical predictions, the function clearly shows a Schrödinger 'cat' state. It depicts a ring structure with a maximum $W_{max} \approx 0.21$ at $(x,p) \approx (0,-1.9)$ and a negative minimum $W_{min} \approx -0.004$ at $(x,p) \approx (0,-0.8)$. **b**, Contour colour plot of the projected Wigner function on the (x,p) plane.

M. Lewenstein *et. al.*, arXiv/2008.10221 (2020), Nature Phys.17, 1104{1108 (2021).

Quantum nature of EM radiation in strongly laser driven atoms

FORTH
INSTITUTE OF ELECTRONIC STRUCTURE AND LASER

Attosecond Science and Technology group

Th. Lamprou
N. Papadakis
E. Skantzakis
I. Liontos
P. Tzallas





ICFO + UCL + Guangdong Technion + Aarhus

M. Lewenstein
J. Rivera-Dean
M. F. Ciappina
E. Pisanty,
Ph. Stammer
A. Maxwell
A. Ordóñez

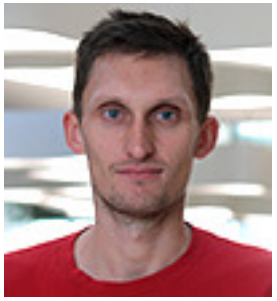


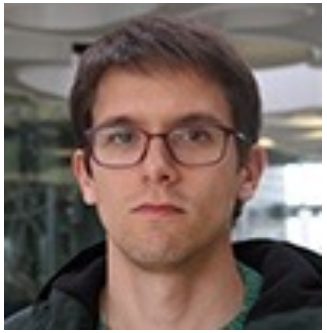


5. Generalizations: Conditioning on…

6.1 – Conditioning on ATI (direct tunelling)

Light-matter entanglement after above-threshold ionization processes in atoms

J. Rivera-Dean,[1,*] P. Stammer,[1] A. S. Maxwell,[2] Th. Lamprou,[3,4] P. Tzallas,[3,5] M. Lewenstein,[1,6] and M. F. Ciappina[7,8,9,†]

[1]*ICFO – Institut de Ciencies Fotoniques, The Barcelona Institute of Science and Technology, 08860 Castelldefels (Barcelona)*
[2]*Department of Physics and Astronomy, Aarhus University, DK-8000 Aarhus C, Denmark*
[3]*Foundation for Research and Technology-Hellas, Institute of Electronic Structure & Laser, GR-70013 Heraklion (Crete), Greece*
[4]*Department of Physics, University of Crete, P.O. Box 2208, GR-70013 Heraklion (Crete), Greece*
[5]*ELI-ALPS, ELI-Hu Non-Profit Ltd., Dugonics tér 13, H-6720 Szeged, Hungary*
[6]*ICREA, Pg. Lluís Companys 23, 08010 Barcelona, Spain*
[7]*Physics Program, Guangdong Technion–Israel Institute of Technology, Shantou, Guangdong 515063, China*
[8]*Technion – Israel Institute of Technology, Haifa, 32000, Israel*
[9]*Guangdong Provincial Key Laboratory of Materials and Technologies for Energy Conversion, Guangdong Technion – Israel Institute of Technology, Shantou, Guangdong 515063, China*

(Dated: August 29, 2022)

Light-matter entanglement plays a fundamental role in many applications of quantum information science. Thus, finding processes where it can be observed is an important task. Here, we address this matter by theoretically investigating the entanglement between light and electrons generated in above-threshold ionization (ATI) process. The study is based on the back-action of the ATI process on the quantum optical state of the system, and its dependence on the kinetic energy and direction of the emitted photoelectrons. Taking into account the dynamics of the process, we demonstrate the creation of hybrid entangled states. The amount of entanglement has been studied in terms of the entropy of entanglement. Additionally, we use the Wigner function of the driving field mode to motivate the entanglement characterization when considering electrons propagating in opposite directions.

26 Aug 2022

6.1 – Conditioning on ATI (direct tunelling)

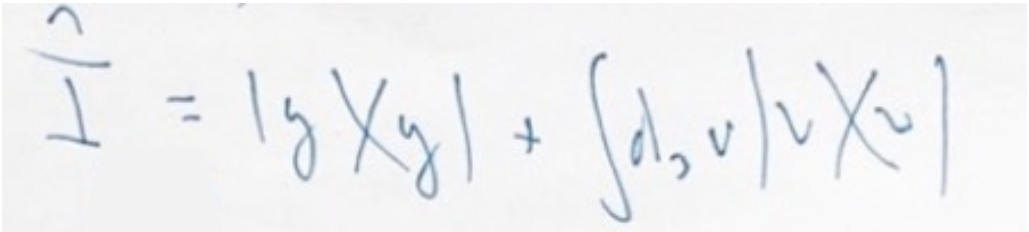

$$|\psi(t)\rangle = e^{-\frac{i}{\hbar}I_p(t-t_0)}|\mathrm{g}\rangle|\bar{0}\rangle - \frac{i}{\hbar}\int \mathrm{d}^3\mathbf{p}\int_{t_0}^{t}\mathrm{d}t' e^{-\frac{i}{\hbar}S(\mathbf{p},t,t')}\tilde{D}(\delta(\mathbf{p},t,t'))(\mathbf{E}_{\mathrm{cl}}(t')+\hat{\mathbf{E}}(t'))\cdot\mathbf{d}\left(\mathbf{p}+\frac{e}{c}\mathbf{A}(t')\right)\left|\mathbf{p}+\frac{e}{c}\mathbf{A}(t)\right\rangle|\bar{0}\rangle, \quad (9)$$

where $\mathbf{v} = \mathbf{p} + (e/c)\mathbf{A}(t)$ with $\mathbf{p}$ the canonical momentum, $\mathbf{d}(\mathbf{p}+(e/c)\mathbf{A}(t)) \equiv \langle \mathbf{p}+(e/c)\mathbf{A}(t)|\hat{\mathbf{R}}|\mathrm{g}\rangle$, $S(\mathbf{p},t,t')$ is the semi-classical action

$$S(\mathbf{p},t,t') = \int_{t'}^{t}\mathrm{d}\tau\left(\frac{1}{2m}\left[\mathbf{p}+\frac{e}{c}\mathbf{A}(\tau)\right]^2 + I_p\right), \quad (10)$$

with I_p the ionization potential of the considered atom, and where

$$\tilde{D}(\delta(\mathbf{p},t,t')) = \prod_{\mathbf{k},\mu} e^{i\varphi_{\mathbf{k},\mu}(\mathbf{p},t)} D(\delta_{\mathbf{k},\mu}(\mathbf{p},t,t')). \quad (11)$$

time t' up to the final time t. Both quantities are explicitly given by

$$\delta_{\mathbf{k},\mu}(\mathbf{p},t,t') = -\frac{e}{\hbar}\sqrt{\frac{\hbar\omega_k}{2\epsilon_0 V}}\int_{t'}^{t}\mathrm{d}\tau\Delta\mathbf{r}(\mathbf{p},\tau,t')e^{i\omega_k\tau}, \quad (12)$$

$$\varphi_{\mathbf{k},\mu}(\mathbf{p},t) = \frac{e^2}{\hbar^2}\frac{\hbar\omega_k}{2\epsilon_0 V}\int_{t'}^{t}\mathrm{d}t_1\int_{t'}^{t_1}\mathrm{d}t_2\left(\epsilon_{\mathbf{k},\mu}\cdot\Delta\mathbf{r}(\mathbf{p},t_1,t')\right) \times\left(\epsilon_{\mathbf{k},\mu}\cdot\Delta\mathbf{r}(\mathbf{p},t_2,t')\right) \times\sin(\omega_k(t_1-t_2)). \quad (13)$$

ICFO
Institut de Ciències Fotòniques

6.1 – Conditioning on ATI (direct tunelling)

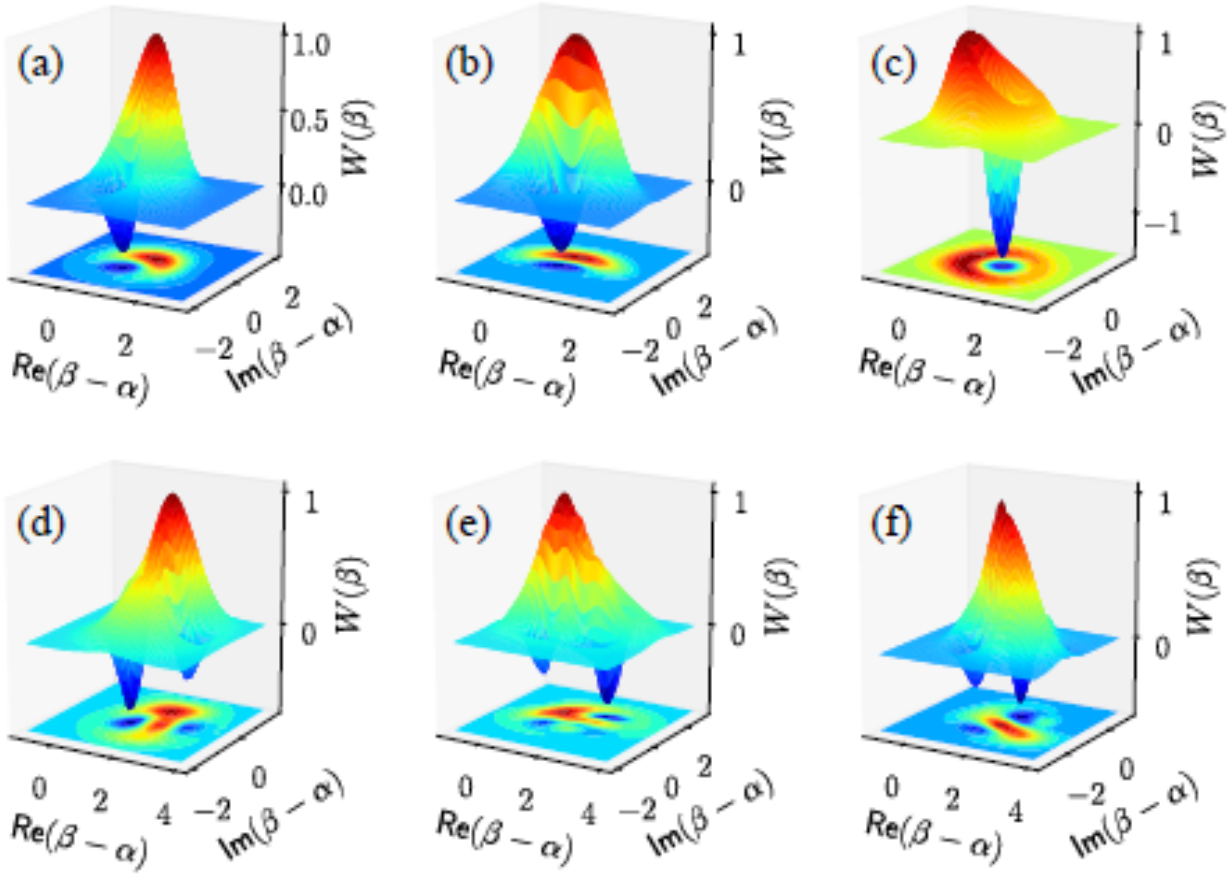

FIG. 5. Wigner function of the state shown in Eq. (24). In the first row (plots (a)–(c)), we have set $N \sim 10^4$ atoms while in the second row (plots (d)–(f)) we have used $N \sim 2 \times 10^4$. Each of the columns correspond to different values of the employed canonical momentum. In particular, we have used $p = 0.00$ a.u. (plots (a) and (d)), $p = 0.43$ a.u. (plots (b) and (e)) and $p = -0.43$ a.u. (plots (c) and (f)). For the numerical calculations we have used a linearly polarized electromagnetic field with a sinusoidal squared envelope of 5 cycles of duration, $E_0 = 0.053$ a.u. for the field's amplitude, $\omega_L = 0.057$ a.u. for the central frequency. For the atomic system, we used a 1D model of Hydrogen with $I_p = 0.5$ a.u. for the ionization potential. We have set in our calculations the final time to coincide with the end of the pulse. Furthermore, we have normalized the results to the maximum value found for the Wigner function. More details about the generation of the Wigner plots can be found in Appendix C 3.

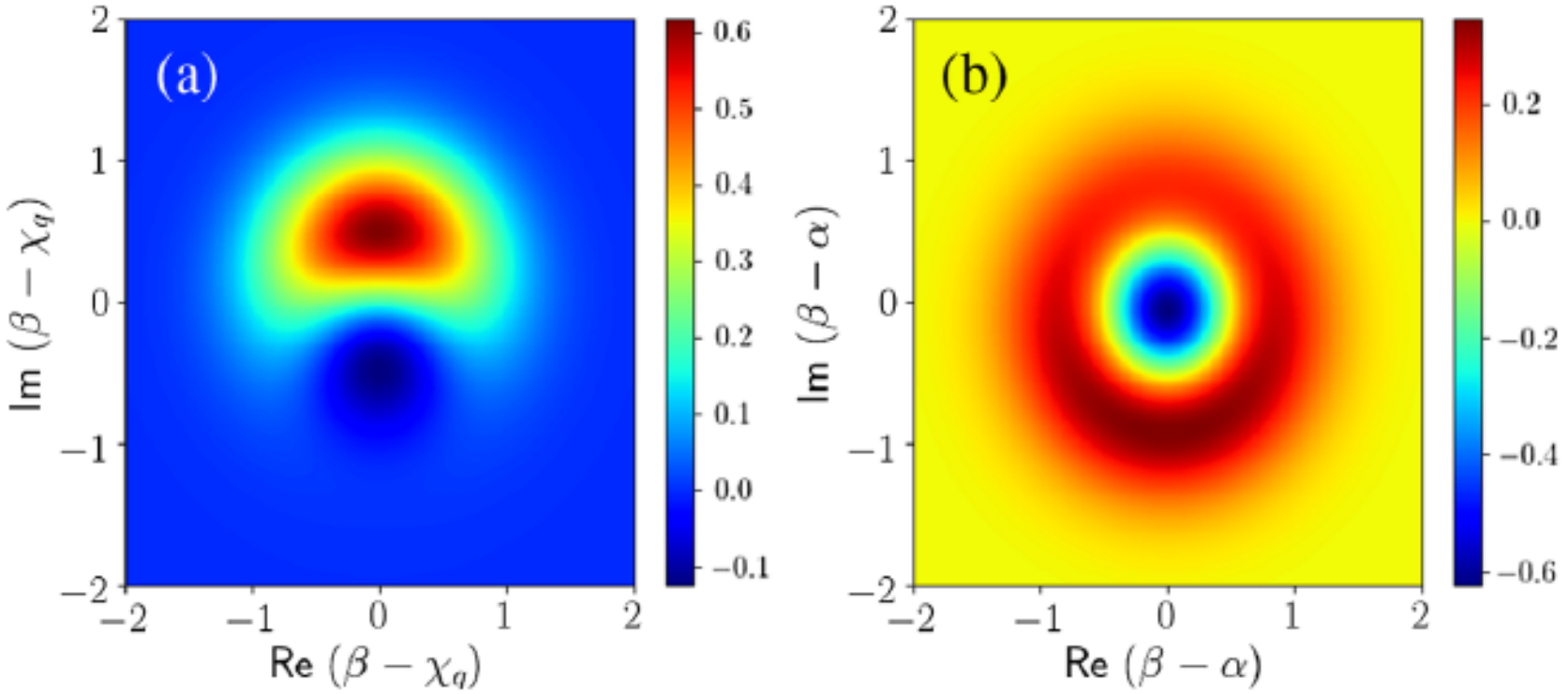

FIG. 2. Wigner function of the coherent state superposition (a) of the qth harmonic Eq. (6) and (b) of the fundamental mode corresponding to Eq. (3). The calculation has been performed using $\delta\alpha = -0.2$, such that $\chi_q \approx 0.03$ for a harmonic cutoff $N = 11$. The opposite shift in imaginary part reflects the correlation between the field modes.

6.3 – Light-matter entanglement in solids

ICFO Institut de Ciències Fotòniques

Creation of entangled and non-classical states of light in strong-laser driven semiconductors

J. Rivera-Dean,[1,*] P. Stammer,[1] A. S. Maxwell,[2] Th. Lamprou,[3,4] A. F. Ordóñez,[1] E. Pisanty,[5] P. Tzallas,[3,6] M. Lewenstein,[1,7,†] and M. F. Ciappina[8,9,10,‡]

[1] *ICFO – Institut de Ciencies Fotoniques, The Barcelona Institute of Science and Technology, 08860 Castelldefels (Barcelona)*
[2] *Department of Physics and Astronomy, Aarhus University, DK-8000 Aarhus C, Denmark*
[3] *Foundation for Research and Technology-Hellas, Institute of Electronic Structure & Laser, GR-70013 Heraklion (Crete), Greece*
[4] *Department of Physics, University of Crete, P.O. Box 2208, GR-70013 Heraklion (Crete), Greece*
[5] *Department of Physics, King's College London, WC2R 2LS London, United Kingdom*
[6] *ELI-ALPS, ELI-Hu Non-Profit Ltd., Dugonics tér 13, H-6720 Szeged, Hungary*
[7] *ICREA, Pg. Lluís Companys 23, 08010 Barcelona, Spain*
[8] *Physics Program, Guangdong Technion–Israel Institute of Technology, Shantou, Guangdong 515063, China*
[9] *Technion – Israel Institute of Technology, Haifa, 32000, Israel*
[10] *Guangdong Provincial Key Laboratory of Materials and Technologies for Energy Conversion, Guangdong Technion – Israel Institute of Technology, Shantou, Guangdong 515063, China*

(Dated: March 20, 2023)

Non-classical states of light are essential for optical quantum information science. We demonstrate the generation of such states using high-order harmonic generation in solid-state systems when driven with strong-laser fields. The electron recombination in the solid determines how the electromagnetic field gets affected after the laser-matter interaction, leading to entanglement between the electron and the field. We also apply conditioning operations based on high-harmonic radiation measurement to enhance these features. Our work lays the foundation for compact solid-state-based non-classical light sources using strong-field physics.

The next step is to go to the interaction picture with respect to $\hat{H}_{sc}(t)$, something that we achieve with the following transformation

$$|\Psi(t)\rangle = \mathcal{T} \exp\left[-\mathrm{i}\int_0^t \hat{H}_{sc}(t')\mathrm{d}t'/\hbar\right]|\psi(t)\rangle\,, \tag{10}$$

where $\mathcal{T}$ denotes the time-ordered product. Then we obtain:

$$\mathrm{i}\hbar\frac{\partial}{\partial t}|\psi(t)\rangle = -e\hat{\mathbf{E}}_{Q}(t)\cdot\hat{\mathbf{r}}_{H}(t)\,|\psi(t)\rangle\,. \tag{11}$$

The transformation depicted in equation (10) does not alter the initial condition for the system, but introduces in our Schrödinger equation the dynamics

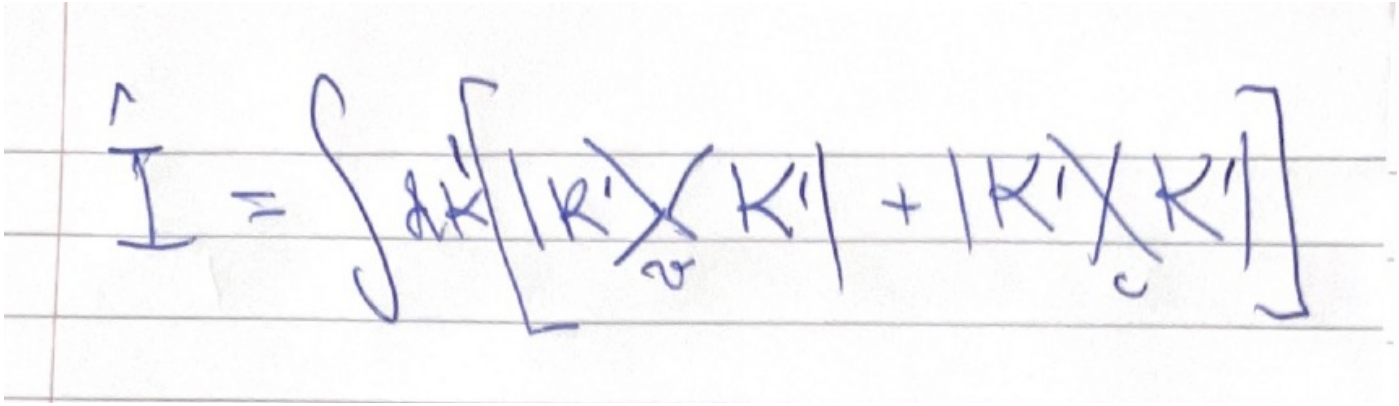

6.3 Unitaries for solids

$$\hat{I} = \int_{(1)} dk' \left[|k'\rangle_v \langle k'| + |k'\rangle_c \langle k'| \right]$$

$$i\hbar \frac{\partial}{\partial t} {}_v\langle k|\psi(t)\rangle =$$

$$= -e \hat{E}_q(t) \, {}_v\langle k|\hat{r}_H(t)|\psi(t)\rangle$$

$$\sum_{v'} {}_v\langle k|\hat{r}_H(t)|k'\rangle_{v'}$$

$${}_v\langle k+A(t)|\hat{r}_{H,q}(t)|k'+A(t)\rangle_{v'}$$

$$= {}_v\langle k+A(t)|\hat{r}_{H,q}(t)|k+A(t)\rangle_{v'} \cdot \delta(k-k')$$

6.3 Unitaries for solids

$$\hat{I} = \int d\vec{k} \left[|k\rangle_v \langle k| + |k\rangle_c \langle k| \right]$$

So, neglecting conduction band, we get

$$i\hbar \frac{\partial}{\partial t} \langle k|\psi(t)\rangle = -\vec{E}(t) \langle k|r_H(t)|k\rangle \langle k|\psi(t)\rangle$$

6.3 - Light-matter entanglement in solids

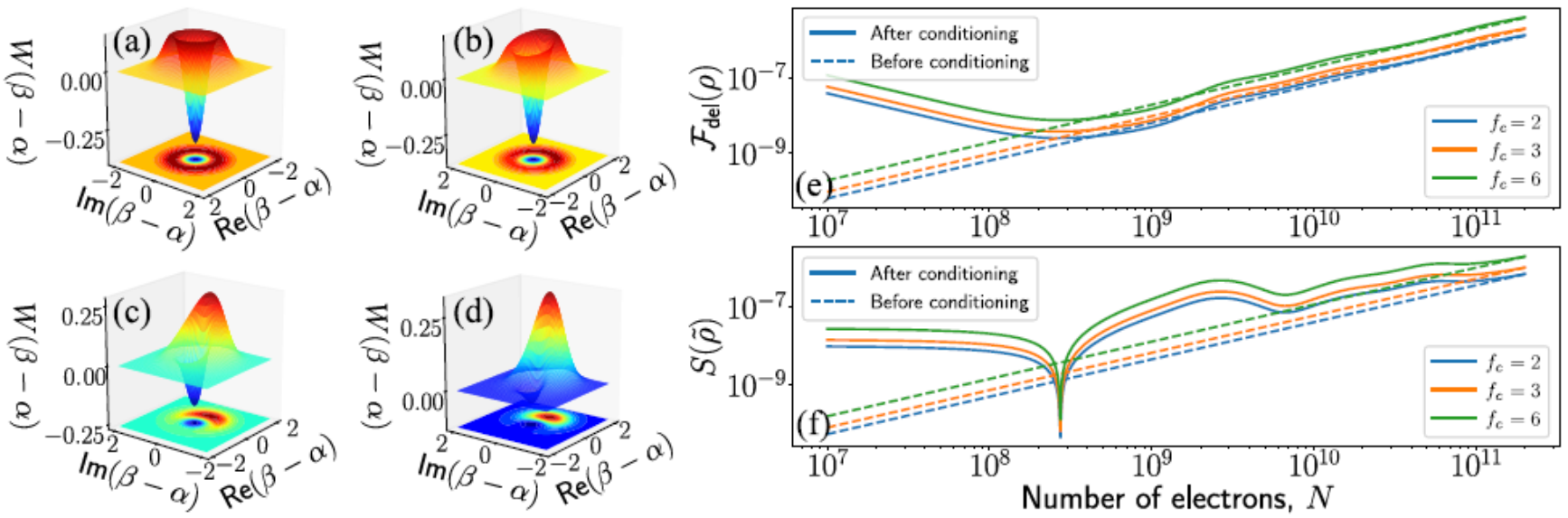

FIG. 2. **Wigner function representation, fidelity and entanglement for the many-electron case.** In (a) to (d), we show the Wigner function distribution of the state after the conditioning for different values of N, specifically (a) $N = 1 \times 10^7$, (b) $N = 1 \times 10^8$, (c) $N = 5 \times 10^8$ and (d) $N = 1 \times 10^9$. We have used the terminology presented in Ref. [48], such that $\mathrm{Re}(\beta - \alpha) = x$ and $\mathrm{Im}(\beta - \alpha) = p$ with x and p are the mean value of the quadrature operators $\hat{p} = (\hat{a} - \hat{a}^\dagger)/(i\sqrt{2})$ and $\hat{x} = (\hat{a} + \hat{a}^\dagger)/\sqrt{2}$. In (e) and (f) we show, respectively, the fidelity of the state in Eq. (7) with respect to the state $|w_{v,\overline{\mathrm{NN}}}\rangle$, and the entropy of entanglement $S(\tilde{\rho})$, with $\tilde{\rho} = \mathrm{tr}_{\mathrm{field}}(|\psi(t)\rangle\langle\psi(t)|)$ for the dashed curves and $\tilde{\rho} = \mathrm{tr}_{\mathrm{field}}(|\Psi_{\mathrm{cond}}(t)\rangle\langle\Psi_{\mathrm{cond}}(t)|)$ for the solid curves, when considering different coordinate numbers f_c, which correspond to a 1D lattice ($f_c = 2$ in blue), a honeycomb lattice in 2D ($f_c = 3$ in orange) and a triangular lattice in 2D ($f_c = 6$ in green). In both plots, we consider the state before and after the conditioning operation is applied, which are respectively shown with the dashed and solid curves, respectively.

6.4 – Detection of cat/kitten states

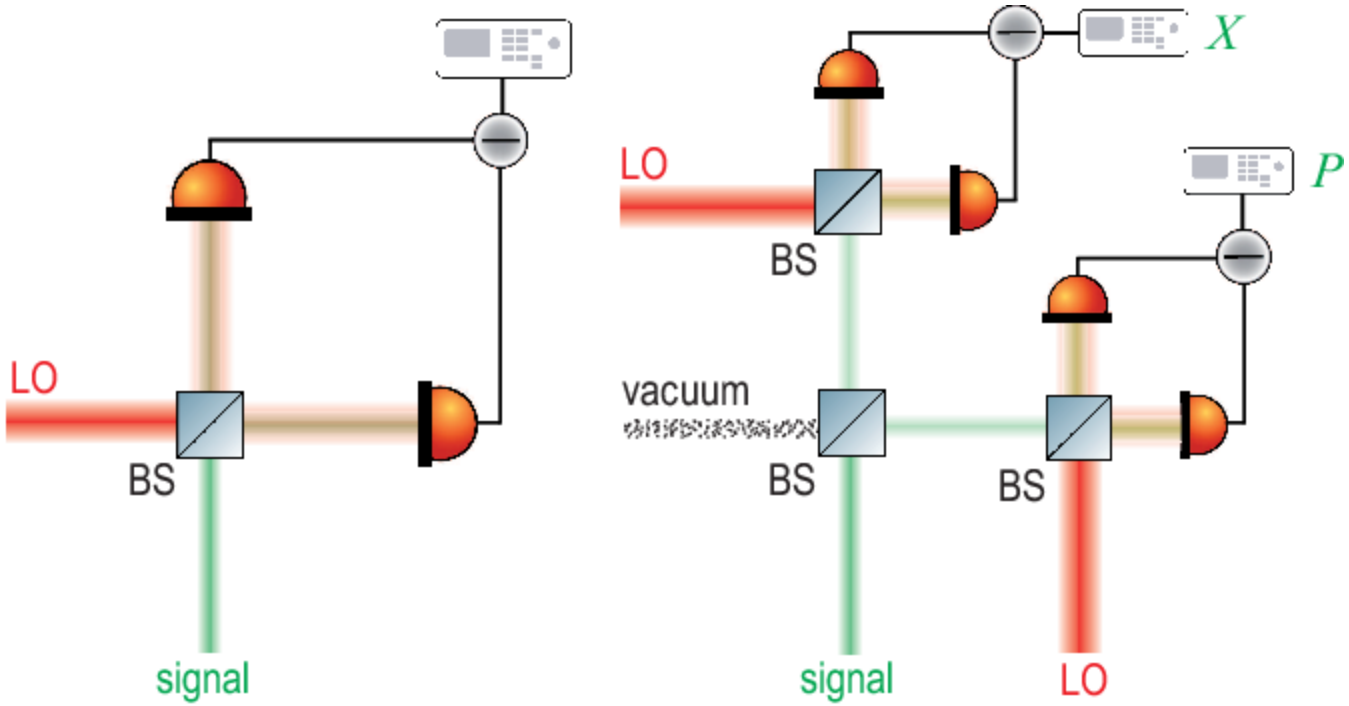

From: Superiority of heterodyning over homodyning: An assessment with quadrature moments, Y.S. Teo, *et al.*, PRA (2017).

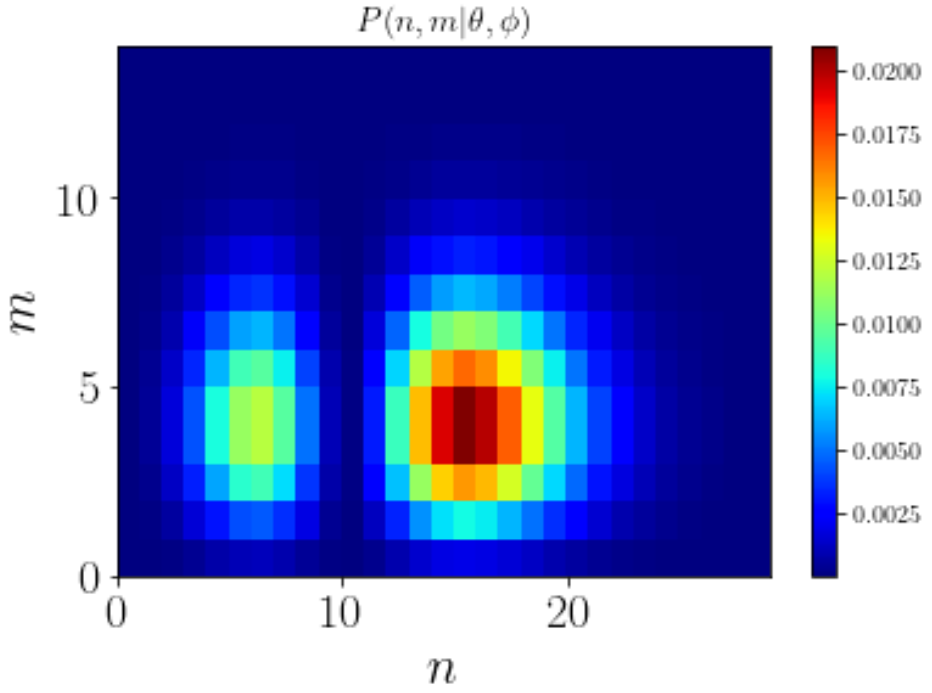

OUR CAT HOMODYNED WITH BETA

alpha = 3.0,
delta alpha = 0.5,
beta = 2.0,

OUR CAT HOMODYNED WITH BETA AND BEAM SPLITTED

alpha = 3.0,
delta alpha = 0.5,
beta = 2.0,
theta = pi/4,
phi = pi/2

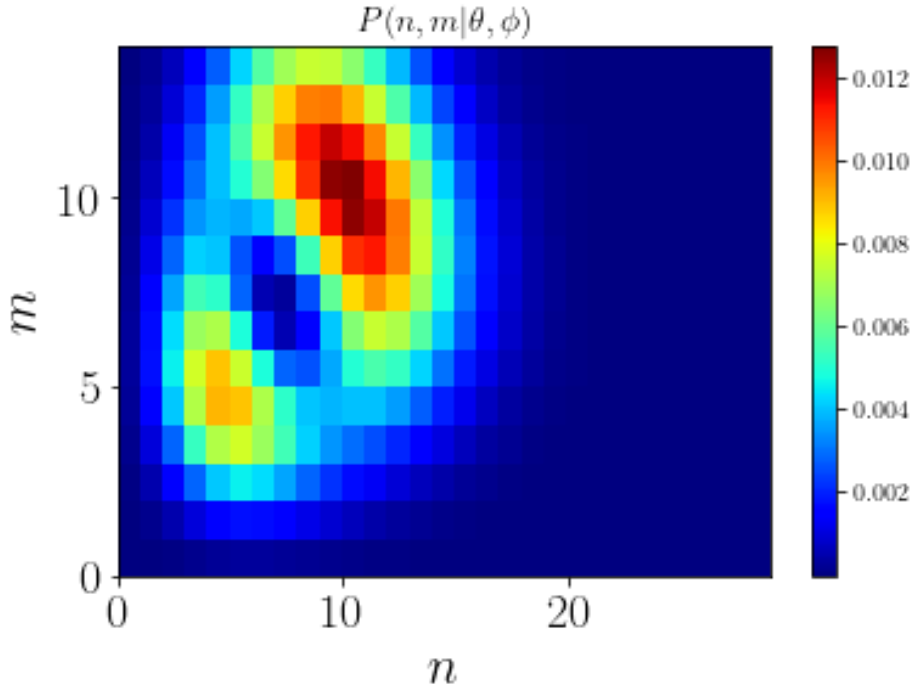

Tutorial

Quantum Electrodynamics of Intense Laser-Matter Interactions: A Tool for Quantum State Engineering

Philipp Stammer,[1,*] Javier Rivera-Dean,[1] Andrew Maxwell,[1,2] Theocharis Lamprou,[3,4] Andrés Ordóñez,[1] Marcelo F. Ciappina,[5,6,7] Paraskevas Tzallas,[3,8] and Maciej Lewenstein[1,9]

[1] *ICFO-Institut de Ciencies Fotoniques, The Barcelona Institute of Science and Technology, Castelldefels, Barcelona 08860, Spain*

[2] *Department of Physics and Astronomy, Aarhus University, Aarhus C DK-8000, Denmark*

[3] *Foundation for Research and Technology-Hellas, Institute of Electronic Structure & Laser, Heraklion, Crete GR-70013, Greece*

[4] *Department of Physics, University of Crete, P.O. Box 2208, Heraklion, Crete GR-71003, Greece*

[5] *Physics Program, Guangdong Technion—Israel Institute of Technology, Shantou, Guangdong 515063, China*

[6] *Technion—Israel Institute of Technology, Haifa 32000, Israel*

[7] *Guangdong Provincial Key Laboratory of Materials and Technologies for Energy Conversion, Guangdong Technion—Israel Institute of Technology, Shantou, Guangdong 515063, China*

[8] *ELI-ALPS, ELI-Hu Non-Profit Ltd., Dugonics tér 13, Szeged, H-6720 Hungary*

[9] *ICREA, Pg. Lluis Companys 23, Barcelona 08010, Spain*

(Received 30 June 2022; published 20 January 2023)

Intense laser-matter interactions are at the center of interest in research and technology since the development of high-power lasers. They have been widely used for fundamental studies in atomic, molecular, and optical physics, and they are at the core of attosecond physics and ultrafast optoelectronics. Although the majority of these studies have been successfully described using classical electromagnetic fields, recent investigations based on fully quantized approaches have shown that intense laser-atom interactions can be used for the generation of controllable high-photon-number entangled coherent states and coherent state superpositions. In this tutorial, we provide a comprehensive fully quantized description of intense laser-atom interactions. We elaborate on the processes of high-harmonic generation, above-threshold ionization, and we discuss new phenomena that cannot be revealed within the context of semiclassical theories. We provide the description for conditioning the light field on different electronic processes, and their consequences for quantum state engineering of light. Finally, we discuss the extension of the approach to more complex materials, and the impact to quantum technologies for a new photonic platform composed of the symbiosis of attosecond physics and quantum information science.

DOI: 10.1103/PRXQuantum.4.010201

Moon-shot research projects

ICFO Institut de Ciències Fotòniques

Attophysics for GENERATION and APPLICATIONS of massively quantum correlated states etc. (13 papers, 4 in pipeline)

1) Theocharis Lamprou, Rodrigo Lopez-Martens Rodrigo, Stefan Haessler, Ioannis Liontos, Subhendu Kahaly, Javier Rivera-Dean, Philipp Stammer, Emilio Pisanty, Marcelo Ciappina, Maciej Lewenstein, Paraskevas Tzallas, Quantum-optical spectrometry in relativistic laser-plasma interactions using the high-harmonic generation process: A proposal, Photonics 8(6), 192 (2021), arXiv:2106.00372, https://doi.org/10.3390/photonics8060192.

2) Maciej Lewenstein, Marcelo F. Ciappina, Emilio Pisanty, Javier Rivera-Dean, Theocharis Lamprou, and Paraskevas Tzallas, Generation of optical Schrödinger cat states in intense laser-matter interactions (title in arXiv:The quantum nature of light in high harmonic generation), Nature Phys. 17, 1104–1108, (2021), https://doi.org/10.1038/s41567-021-01317-w, arXiv:2008.10221.

3) Javier Rivera-Dean, Philipp Stammer, Emilio Pisanty, Theocharis Lamprou, Paraskevas Tzallas, Maciej Lewenstein, and Marcelo F. Ciappina, New schemes for creating large optical Schrodinger cat states using strong laser fields, arXiv:2107.12811, J. Comp. Elec. 20, 2111 (2021), https://doi.org/10.1007/s10825-021-01789-2.

4) Philipp Stammer, Javier Rivera-Dean, Theocharis Lamprou, Emilio Pisanty, Marcelo F. Ciappina, Paraskevas Tzallas, and Maciej Lewenstein, High photon number entangled states and coherent state superposition from the extreme-ultraviolet to the far infrared, Phys. Rev. Lett. 128, 123603 (2022), arXiv:2107.12887.

5) Javier Rivera-Dean, Theocharis Lamprou, Emilio Pisanty, Philipp Stammer, Andrés F. Ordóñez, Marcelo F. Ciappina, Maciej Lewenstein, and Paraskevas Tzallas, Quantum optics of strongly laser--driven atoms and generation of high photon number optical cat states, Phys. Rev. A 105, 033714 (2022).

6) Philipp Stammer, Javier Rivera-Dean, Andrew Maxwell, Theocharis Lamprou, Andres Ordóñez, Marcelo F. Ciappina, Paraskevas Tzallas, and Maciej Lewenstein, Quantum electrodynamics of ultra-intense laser-matter interactions, invited tutorial for Phys. Rev. X 4, 010201 (2023), arXiv:2206.04308.

6) Philipp Stammer, Theory of entanglement and measurement in high harmonic generation, Phys. Rev. A 106, L050402 (2022), arXiv:2203.04354

7) Javier Rivera-Dean, Philipp Stammer, Andrew S. Maxwell, Theocharis Lamprou, Paraskevas Tzallas, Maciej Lewenstein, and Marcelo F. Ciappina, Light-matter entanglement after above-threshold ionization processes in atoms, arXiv:2208.05245v1, Phys. Rev. A 106, 063705 (2022).

8) M. Lewenstein, N. Baldelli, U. Bhattacharya, J. Biegert, M. F. Ciappina, U. Elu, T. Grass, P. T. Grochowski, A. Johnson, Th. Lamprou, A. S. Maxwell, A. Ordóñez, E. Pisanty, J. Rivera-Dean, P. Stammer, I. Tyulnev, and P. Tzallas, Attosecond Physics and Quantum Information Science, Proceeding of ATTOVIII, Eds. L. Argenti, M. Chini, and L. Fang, arXiv:2208.14769v1.

9) Javier Rivera-Dean, Philipp Stammer, Andrew S. Maxwell, Theocharis Lamprou, Andrés F. Ordóñez, Emilio Pisanty, Paraskevas Tzallas, Maciej Lewenstein, and Marcelo F. Ciappina, Quantum optical engineering in strong-laser driven semiconductors: A protocol for developing non-classical light sources, with referees in Phys. Rev. Lett., arXiv:2211.00033.

10) Utso Bhattacharya, Theocharis Lamprou, Andrew S. Maxwell, Andrés F. Ordóñez, Emilio Pisanty, Javier Rivera-Dean, Philipp Stammer, Marcelo F. Ciappina, Maciej Lewenstein, and Paraskevas Tzallas, Strong laser physics, non-classical light states and quantum information science, submitted to ROPP, arXiv:2302.04692.

11) Philipp Stammer and Maciej Lewenstein. Quantum Optics as Applied Quantum Electrodynamics is back in town, submitted to Acta Phys. Polon., special issue celebrating 90th birthday of I. Birula-Białynicki, Ed. Tomasz Sowiński, arXiv:2306.07854, Acta Phys. Pol. A 143, S42 (2023).

12) Theocharis Lamprou, Javier Rivera-Dean, Philipp Stammer, Maciej Lewenstein, and Paraskevas Tzallas, Nonlinear optics using intense optical Schrödinger "cat" states, arXiv:2306.14480.

13) J. Rivera-Dean, P. Stammer, A. S. Maxwell, Th. Lamprou, E. Pisanty, P. Tzallas, M. Lewenstein, and M.F. Ciappina, Quantum optical analysis of high-order harmonic generation in H+ molecular ions (preprint in arxivs next week)

Moon-shot research projects

ICFO Institut de Ciències Fotòniques

Attophysics for GENERATION and APPLICATIONS of massively quantum correlated states etc.

Significant others:

FORTH/ICFO collaboration

Technion group (Oren Cohen, Ido Kaminer) - "using quantim light to generate more quantum light"

Jena group (Stefanie Gräfe) "looking at semiconductor intraband excitations"

ICFO group (Jens Biegert) ???

MBI group

Moon-shot research projects

Attophysics for DETECTION of topology, strongly correlated systems, chirality etc. (5 papers, 2 in pipeline)

1) Alexis Chacón, Wei Zhu, Shane P. Kelly, Alexandre Dauphin, Emilio Pisanty, Antonio Picón, Christopher Ticknor, Marcelo F. Ciappina, Avadh Saxena, Maciej Lewenstein, Circular dichroism in higher-order harmonic generation: Heralding topological phases and transitions in Chern insulators, Phys. Rev. B 102, 134115 (2020), arXiv:1807.01616.

2) Jordi Alcalà, Utso Bhattacharya, Jens Biegert, Marcelo Ciappina, Ugaitz Elu, Tobias Graß, Piotr T. Grochowski, Maciej Lewenstein, Anna Palau, Themistoklis P. H. Sidiropoulos, Tobias Steinle, and Igor Tyulnev, High harmonic spectroscopy of quantum phase transitions in a high-T_c superconductor, PNAS 119 (40) e2207766119 (2022), arXiv:2201.09515.

3) Niccolò Baldelli, Utso Bhattacharya, Daniel González-Cuadra, Maciej Lewenstein, and Tobias Graß, Detecting Majorana Zero Modes via Strong Field Dynamics, ACS Omega 7 (50), 47424–47430 (2022), arXiv:2202.03547v1.

4) Xavier Barcons Planas, Andrés Ordóñez, Maciej Lewenstein, and Andrew Stephen Maxwell, Strong-field chiral imaging with twisted photoelectrons, Phys. Rev. Lett. 129, 233201 (2022), arXiv:2202.07289.

- 5) Mohit Lal Bera, Jessica O. de Almeida, Marlena Dziurawiec, Marcin Płodzień, Maciej M. Maśka, Maciej Lewenstein, Tobias Grass, and Utso Bhattacharya, Topological phase detection through high-harmonic spectroscopy in extended Su-Schrieffer-Heeger chains,
- arXiv:2305.02025.

- Two more papers with MARLENA DZIURAWIEC - Talk to her!

ICFO Institut de Ciències Fotòniques

Moon-shot research projects

ICFO Institut de Ciències Fotòniques

Attophysics for DETECTION of topology, strongly correlated systems, chirality etc.

Significant others:

FORTH/ICFO collaboration

MBI group (Olga Smirnova, Misha Ivanov)

Dieter Bauer

ICFO groups (Jens Biegert, Maciej Lewenstein)

Moon-shot research projects

Attophysics for GENERATION of topology, strongly correlated systems, chirality etc. (6 papers, 2 in pipeline)

1) Utso Bhattacharya, Swati Chaudhary, Tobias Graß, A. Johnson, S. Wall, and Maciej Lewenstein, arXiv:2006.10688, Fermionic Chern insulator from twisted light with linear polarization, Phys. Rev. B 105, L081406 (2022).

2) T.A. Miller, R. W. Chhajlany, L. Tagliacozzo, B. Green, S. Kovalev, D. Prabhakaran, M. Lewenstein, M. Gensch, and S. Wall, Terahertz field control of in-plane orbital order in $La_{0.5}Sr_{1.5}MnO_4$, Nature Commun. 6, 8175 (2015), arXiv:1506.01546.

3) Sergi Julià-Farré, Alexandre Dauphin, Ravindra W. Chhajlany, Piotr T. Grochowski, Simon Wall, Maciej Lewenstein, and Przemysław R. Grzybowski, Nanoscale phase separation and pseudogap in the hole-doped cuprates from fluctuating Cu-O-Cu bonds, Phys. Rev. B 101, 125107 (2020), arXiv:1909.02482.

4) Emilio Pisanty, Gerard Jiménez, Verónica Vicuña-Hernández, Antonio Picón, Alessio Celi, Juan P. Torres, Maciej Lewenstein, Knotting fractional-order knots with the polarization state of light, arXiv:1808.05193, Nature Photonics 13, 569 (2019), doi:10.1038/s41566-019-0450-2 (2019).

5) Emilio Pisanty, Laura Rego, Julio San Román, Antonio Picón, Kevin M. Dorney, Henry C. Kapteyn, Margaret M. Murnane, Luis Plaja, Maciej Lewenstein, and Carlos Hernández-García, Conservation of torus-knot angular momentum in high-order harmonic generation, Phys. Rev. Lett. 122, 203201 (2019), arXiv:1810.06503.

6) Laura Rego, Kevin M. Dorney, Nathan J. Brooks, Quynh Nguyen, Chen-Ting Liao, Julio San Román, David E. Couch, Allison Liu, Emilio Pisanty, Maciej Lewenstein, Luis Plaja, Henry C. Kapteyn, Margaret M. Murnane, Carlos Hernández-García, Light with a self-torque: extreme-ultraviolet beams with time-varying orbital angular momentum, Science 364, eaaw9486 (2019), https://doi.org/10.1126/science.aaw9486, arXiv:1901.10942.

ICFO Institut de Ciències Fotòniques

Moon-shot research projects

Attophysics for GENERATION of topology, strongly correlated systems, chirality

Significant others:

ICFO/IMDEA collaboration

MBI group (Olga Smirnova, Misha Ivanov)

Standard THz suspects (A. Cavalleri, …)

Moon-shot research projects

ICFO Institut de Ciències Fotòniques

Attophysics for GENERATION and APPLICATIONS of entangled states in Zerfall processes etc. (2 papers, 2 in pipeline)

1) Andrew S. Maxwell, Lars Bojer Madsen, and Maciej Lewenstein, Entanglement of Orbital Angular Momentum in Non-Sequential Double Ionization, Nature Comm. 13, 4706 (2022), arXiv:2111.10148
2) A. S. Maxwell, G. S. J. Armstrong, M. F. Ciappina, E. Pisanty, Y. Kang, A. C. Brown, M. Lewenstein, and C. Figueira de Morisson Faria, Manipulating Twisted Electrons in Strong-Field Ionization, arXiv:2010.08355, Faraday Discussions 228, 394-412, DOI: 10.1039/D0FD00105H (2021).

An absolute pioneer is Mark Vrakking, as we heard on Monday

Pascal Salières and Charles Bourassin-Bouchet

Anne L´Huillier's group

Femtosecond pulse parameter estimation from photoelectron momenta using machine learning

Tomasz Szołdra,[1,2,*] Marcelo F. Ciappina,[3,4,5] Nicholas Werby,[6,7] Philip H. Bucksbaum,[6,7,8] Maciej Lewenstein,[9,10] Jakub Zakrzewski,[2,11] and Andrew S. Maxwell[12]

[1] *Doctoral School of Exact and Natural Sciences, Jagiellonian University, Łojasiewicza 11, PL-30-348 Kraków, Poland*
[2] *Instytut Fizyki Teoretycznej, Wydział Fizyki, Astronomii i Informatyki Stosowanej, Uniwersytet Jagielloński, Łojasiewicza 11, PL-30-348 Kraków, Poland*
[3] *Department of Physics, Guangdong Technion - Israel Institute of Technology, 241 Daxue Road, Shantou, Guangdong, China, 515063*
[4] *Technion - Israel Institute of Technology, Haifa, 32000, Israel*
[5] *Guangdong Provincial Key Laboratory of Materials and Technologies for Energy Conversion, Guangdong Technion - Israel Institute of Technology, 241 Daxue Road, Shantou, Guangdong, China, 515063*
[6] *Stanford PULSE Institute, SLAC National Accelerator Laboratory 2575 Sand Hill Road, Menlo Park, CA 94025, USA*
[7] *Department of Physics, Stanford University, Stanford, CA 94305, USA*
[8] *Department of Applied Physics, Stanford University, Stanford, CA 94305, USA*
[9] *ICFO-Institut de Ciencies Fotoniques, The Barcelona Institute of Science and Technology, Av. Carl Friedrich Gauss 3, 08860 Castelldefels (Barcelona), Spain*
[10] *ICREA, Pg. Lluís Companys 23, 08010 Barcelona, Spain*
[11] *Mark Kac Complex Systems Research Center, Jagiellonian University, Łojasiewicza 11, PL-30-348 Kraków, Poland*
[12] *Department of Physics and Astronomy, Aarhus University, DK-8000 Aarhus C, Denmark*

(Dated: March 27, 2023)

Deep learning models have provided huge interpretation power for image-like data. Specifically, convolutional neural networks (CNNs) have demonstrated incredible acuity for tasks such as feature extraction or parameter estimation. Here we test CNNs on strong-field ionization photoelectron spectra, training on theoretical data sets to 'invert' experimental data. Pulse characterization is used as a 'testing ground', specifically we retrieve the laser intensity, where 'traditional' measurements typically leads to 20% uncertainty. We report on crucial data augmentation techniques required to successfully train on theoretical data and return consistent results from experiments, including accounting for detector saturation. The same procedure can be repeated to apply CNNs in a range of scenarios for strong-field ionization. Using a predictive uncertainty estimation, reliable laser intensity uncertainties of a few percent can be extracted, which are consistently lower than those given by traditional techniques. Using interpretability methods can reveal parts of the distribution that are most sensitive to laser intensity, which can be directly associated to holographic interferences. The CNNs employed provide an accurate and convenient ways to extract parameters, and represent a novel interpretational tool for strong-field ionization spectra.






Tomasz Szołdra, Andrew Maxwell, Marcelo Ciappina, Nick Werby, Philip H. Bucksbaum, ML, Jakub Zakrzewski

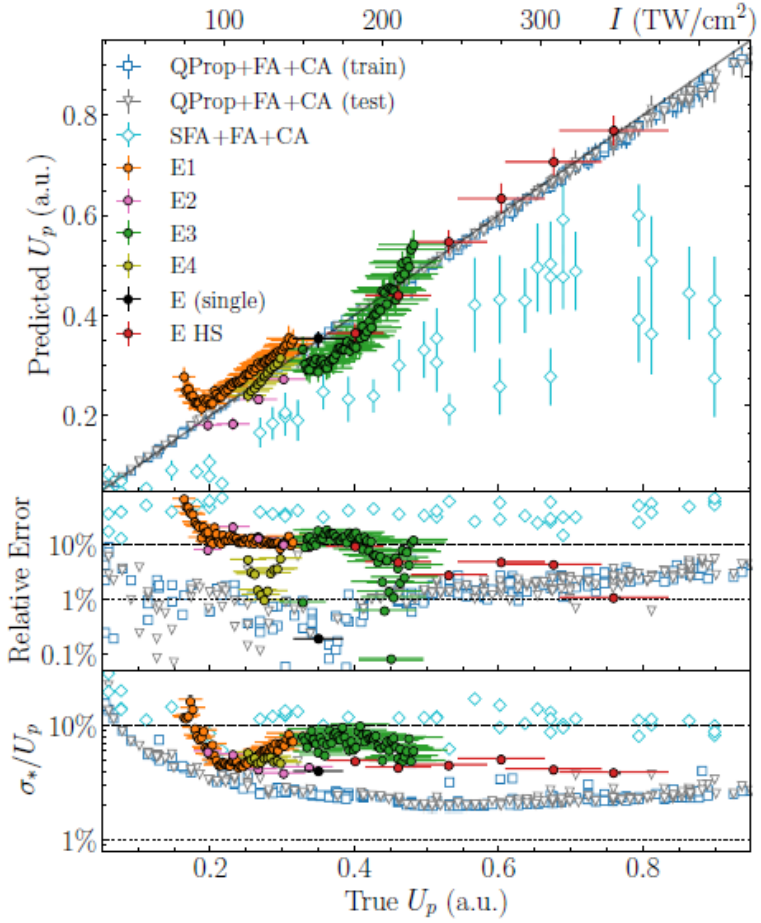

FIG. 3. Performance of the EfficientNetV2L model for training dataset QProp+FA+CA, saturation level $SL = -0.5$, for different test datasets. Top plot shows the value of U_p predicted by the model as a function of the true value. Perfect predictions would lie on the black diagonal line. Including focal- and CEP-averaging in the training dataset was necessary to achieve results in agreement with the experimental value, up to the estimated experimental uncertainty level of 10%, as shown in the middle plot where most experimental points lie below 10% absolute error line. Bottom plot shows a measure of the model confidence, standard deviation $\sigma_\star(U_p)$, as percentage of the true U_p value.

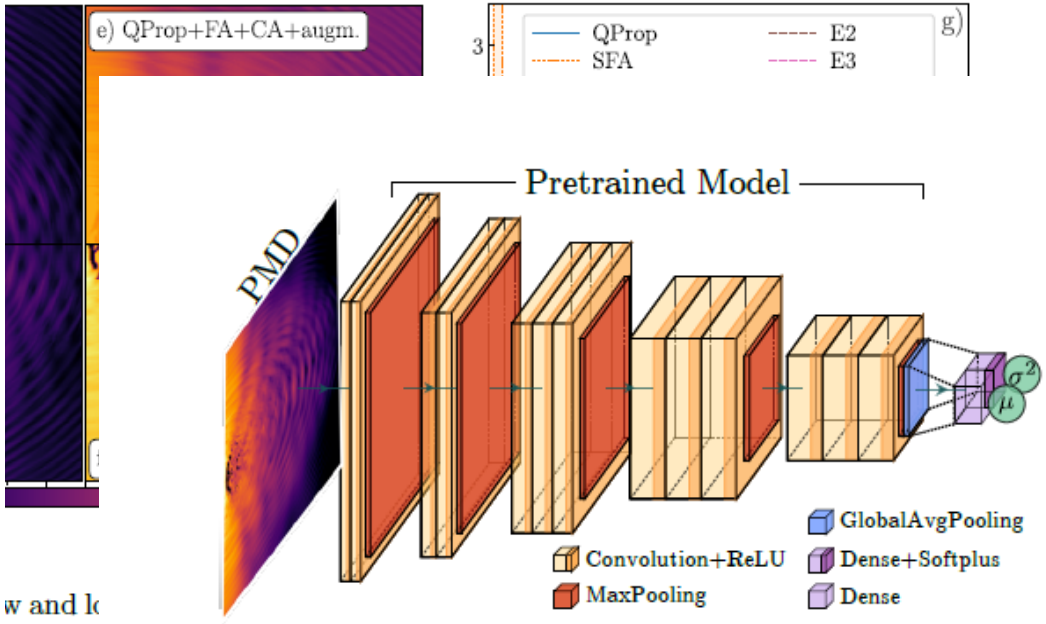

FIG. 2. Schematic representation of the Deep Convolutional Neural Network regression problem. For given input X network predicts the value of the parameter $\mu(X)$ and its uncertainty $\sigma(X)$. Adapted from [60].

w and l
experin
ludes th
MD - mi
ences fr
$SL = 0$
er a ra
ental P

Conclusions

ICFO Institut de Ciències Fotòniques

Conclusions?

Enjoy physics and beyond!!!

*iCrea INSTITUCIÓ CATALANA DE RECERCA I ESTUDIS AVANÇATS

Quantum Narcissism

The Amateur's Guide to Avantgarde:
Catalunya, Poland, Portugal, and
More...

Maciej Lewenstein[1]

April 19, 2021

https://theamateursguidetoavantgarde.bandcamp.com/album/the-amateurs-guide-to-avantgarde





International Journal of Music Science, Technology and Art
(IJMSTA) 3 (2): 17-25, Music Academy "Studio Musica", 2021 ISSN: **2612-2146** (Online)

Ex-assistant of Edgar Varèse

Applications of Quantum Randomness: From Rabi Oscillations to Fourier Axis Controlling the Musical Timbre

Reiko Yamada [1✉], Samuele Grandi [1], Gorka Muñoz-Gil [1], Luca Barbiero [1,3], Albert Aloy [1] and Maciej Lewenstein [1,4✉]

[1]ICFO - Institut de Ciencies Fotoniques, The Barcelona Institute of Science and Technology, Av. Carl Friedrich Gauss 3, 08860 Castelldefels (Barcelona), Spain
[2]Fundació Phonos, Universitat Pompeu Fabra, Roc Boronat 138, 08018, Barcelona, Spain
[3]Institute for Condensed Matter Physics and Complex Systems, DISAT, Politecnico di Torino, I-10129 Torino, Italy
[4]ICREA, Pg. Lluís Companys 23, 08010 Barcelona, Spain
[1]✉ Corresponding author: reiko.yamada@icfo.eu
[1]✉ Corresponding author: maciej.lewenstein@icfo.eu

Andres Lewin-Richter & Vasco Trilla: Sonar 2021

Article Info

Received: January 16, 2021
Accepted: April 02, 2021
Published: August 27, 2021
DOI: https://doi.org/10.48293/IJMSTA-77

Keywords:
Quantum randomness
Rabi oscillation
Musical timbre
Computer-assisted composition

Abstract

Randomness has attracted great interest in the field of music composition for quite some time. As early as 1962, Iannis Xenakis started exploring a stochastic approach to randomness by using computer-based interlinking probability functions to determine compositional structure, pitches and their durations [15]. Soon after, composers and music technologists started to explore randomness with various methods of algorithmic compositions, sometimes with the help of artificial intelligence. However, in most cases, the source of randomness they used was in fact deterministic in nature. That is to say, the random numbers that they employed are imperfect in the strict sense (simply put, perfect random numbers never have repeating patterns). Moreover, the method in which they produced such randomness was extrinsic to the method in which randomness was applied. In this project, we attempt to take a further step by directly producing sound events from the genuine quantum true randomness of quantum physical systems. Through this method, we aim at achieving a new sense of aesthetic effect in music which derives from the true randomness that prevails in the natural quantum world.


SONIFICATION OF THE WIGNER FUNCTION

ICFO
The Institute of Photonic Sciences

Maciej Lewenstein

Reiko Yamada

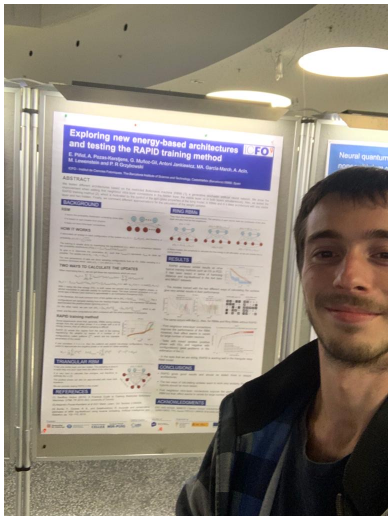

Eloy Piñol Jiménez

An interdisciplinary research project (ICFO, Barcelona) 2022-

7th June
2023

Danish Cultural Institute in Estonia, Latvia and Lithuania and Visionary Culture Foundation, October 15, 2022

Sinfionietta Rīga String Quartet

Koniec

Τέλος